

**A Hardware/Software Platform for Fault Detection and Identification in Electric
Power Distribution Systems for Testing Various Detection Schemes**

A Thesis

Submitted to the Faculty

of

Drexel University

by

Christian M. Schegan

in partial fulfillment of the

requirements for the degree

of

Master of Science in Electrical Engineering

September 2008

© Copyright 2008

Christian M. Schegan. All Rights Reserved.

DEDICATIONS

This thesis is dedicated to my family:
Carl, Terri, Josh, Shirley, Lisa and Dave.

I can never thank you enough
For always believing in me
Encouraging me to persevere
And sticking together as a family
Even through the toughest times.

Without all of your support
I would never be where I am today.

I love you all and thank God
Every day for such a blessing.

ACKNOWLEDGMENTS

I would like to deeply thank my advisor, Dr. Karen Miu, for allowing me to work with her and being so patient while guiding me along in my research. You have always been very honest, teaching me to believe in myself and speak with conviction.

I would like to thank Dr. Niebur for encouraging me to study abroad and providing me with contacts in Germany. You have helped me to do something that I never dreamed I would be able to do and played a great part in one of the best years of my life.

Furthermore I would like to thank Dr. Nwankpa for challenging me so much in the past year. I have really developed a passion for power engineering and teaching because of you.

Lastly I would like to thank Joseph Chunko and Pietro Devine. The two of you are truly the best friends that anyone could ever ask for. You have always been by my side, despite the situation, and provided me with countless hours of comic relief.

TABLE OF CONTENTS

LIST OF TABLES	viii
LIST OF FIGURES	x
CHAPTER 1: Introduction.....	1
1.1 Motivation.....	1
1.2 Background.....	3
1.3 Problem Statement.....	6
1.4 Organization of Thesis.....	7
CHAPTER 2: Review of Fault Analysis Techniques	8
2.1 Review of Fault Analysis.....	8
2.1.1 Fault Detection Using the Discrete Short Time Fourier Transform	10
2.1.2 Wavelet Transform, Filter Banks and Their Application to Fault Analysis	12
2.2 Review of Loading Models and Load Types Used in Fault Analysis	16
2.3 Review of Meter Placement, Measurement Sensitivity and Error.....	16
CHAPTER 3: Problem Formulation	19
3.1 Problem Statement.....	19
3.2 Hardware Platform for Experimentation	20
3.3 Software Platform for Experimentation.....	23
3.4 Load Types and Loading Levels.....	25
3.5 Meter Placement and Measurement Sensitivity.....	26
CHAPTER 4: Solution Methodology	27
4.1 Experiment Design Approach.....	27
4.1.1 Designing an RL Equivalent Motor Load.....	27

4.1.2 Load Distribution for an Unbalanced Radial Distribution System	30
4.1.3 Meter Placement	32
4.2 Wavelet Based Fault Detector Algorithm.....	35
4.2.1 Selecting Threshold Values	35
4.2.2 Load Distributions and Loading Levels.....	38
4.2.3 Measurement Sensitivity.....	39
4.2.4 Wavelets Detector Modifications and Coding.....	40
CHAPTER 5: Experimental Results	44
5.1 Experimental Procedure.....	45
5.2 Overall Performance of the Wavelet Based Fault Detector.....	47
5.2.1 Balanced High Loading Level	48
5.1.2 Unbalanced High Loading Level.....	49
5.1.4 Unbalanced Low Loading Level.....	52
5.1.5 Comparison of Threshold and Detector Accuracy for Each Loading Level	54
5.3 Impacts of Meter Location of Fault Detection and Identification	56
CHAPTER 6: Conclusions.....	60
6.1 Conclusions.....	60
6.2 Summary of Research Contributions.....	61
6.3 Future Work.....	61
BIBLIOGRAPHY	63
Appendix A: Experimental Hardware Setups.....	65
A.1 Experimental Setups Used for Selecting Threshold Values for the Balanced High Loading Level	65

A.2 Experimental Setups Used for Validating Threshold Values for the Balanced High Loading Level	67
A.3 Experimental Setups Used for Selecting Threshold Values for the Unbalanced High, Medium and Low Loading Levels.....	70
A.4 Experimental Setups Used for Validating Threshold Values for the Unbalanced High, Medium and Low Loading Levels.....	73
Appendix B: Flowchart for the Wavelet-Based Fault Detector Code.....	77

LIST OF TABLES

Table 5.1: Threshold values for the balanced High loading level.	48
Table 5.2: Performance errors for the balanced High loading level.	49
Table 5.3: Threshold values for the unbalanced High loading level.	50
Table 5.4: Performance errors for the unbalanced High loading level.	51
Table 5.5: Threshold values for the unbalanced Medium loading level.	51
Table 5.6: Performance errors for the unbalanced Medium loading level.	52
Table 5.7: Threshold values for the unbalanced Low loading level.	53
Table 5.8: Performance errors for the unbalanced Low loading level.	53
Table 5.9: Threshold values selected for all balanced and unbalanced loading levels.	54
Table 5.10: Threshold values for the High and Low loading level were used by the detector for the Low loading level. Measurements were taken at the substation (F).	55
Table 5.11: Overall performance errors for all balanced and unbalanced loading levels.	56
Table 5.12: Bus measurement hardware errors for the balanced High loading level.	58
Table 5.13: Bus measurement hardware errors for the unbalanced High loading level. ..	58
Table 5.14: Bus measurement hardware errors for the unbalanced Medium loading level.	58
Table 5.15: Bus measurement hardware errors for the unbalanced Low loading level.	58
Table A.1: Measurement schemes used for each load distribution in Figure A.1-A.3.	67
Table A.2: Measurement schemes used for the load distribution in Figure A.4.	68
Table A.3: Measurement schemes used for the load distribution in Figure A.9.	70
Table A.4: Measurement schemes used for the load distribution in Figure A.10.	71

Table A.5: Number of light bulbs used per phase for each load in Figure A.13-A.14 for the unbalanced High, Medium and Low loading levels.	72
Table A.6: Number of light bulbs used per phase for each load in Figure A.15 for the unbalanced High, Medium and Low loading levels.	73
Table A.7: Number of light bulbs used per phase for each load in Figure A.16 for the unbalanced High, Medium and Low loading levels.	74

LIST OF FIGURES

Figure 2.1: Three-phase circuit diagram of a Phase A-to-B, LL fault. The fault current for phases a, b, and c are I_{fa} , I_{fb} , and I_{fc} respectively. Z_f is the fault impedance.	9
Figure 2.2: Three-phase circuit diagram of a Phase A-to-B-to-Ground, LLG fault. The fault current for phases a, b, and c are I_{fa} , I_{fb} , and I_{fc} respectively. Z_f is the fault impedance.	10
Figure 2.3: Filter bank representation of the DWT. Here $h[k]$ is a highpass filter, which yields the detail coefficients and $g[k]$ is a lowpass filter, which yields the course signal coefficients [23].	14
Figure 3.1 : One line diagram of RDAC laboratory setup including current limiting protection device [26].	21
Figure 3.2: Over-voltage relays used for fault creation [26].	23
Figure 3.3: VBA GUI for fault creation [26].	24
Figure 4.1: Schematic of a sample load distribution in RDAC, incorporating 1 Φ , 2 Φ and 3 Φ R loads, as well as a 3 Φ RL load.	31
Figure 4.2: Schematic of a common load distribution where one lateral services an industrial client, while the other lateral services residential and commercial customers.	31
Figure 4.3: Sample load distribution where several measurement schemes are possible. Measurement locations are represented by an M above the respective bus.	33
Figure 4.4: Sample load distribution where measurement schemes are limited.	34
Figure 4.5: Output of the wavelet-based algorithm for a LL fault on phases A and C, showing the minimum detail coefficient at fault inception used for selecting threshold values.	36

Figure 4.6: Output of the wavelet-based algorithm for a LL fault on phases B and C, showing a noisy output due to distortion of the voltage waveform.....	37
Figure 4.7: A sample load distribution with measurements at buses F, A4, B1 and B2. A fault occurred at bus B2.....	40
Figure 5.1: A sample load distribution used for experimentation.	46
Figure 5.2: Measurements locations, represented by an M, are then chosen.....	46
Figure 5.3: All 11 fault types are then created at each fault location. Here faults are located at buses A1, B1 and B2.	47
Figure A.1: Configuration 1 for selecting threshold values for the balanced High loading level.....	66
Figure A.2: Configuration 2 for selecting threshold values for the balanced High loading level.....	66
Figure A.3: Configuration 3 for selecting threshold values for the balanced High loading level.....	66
Figure A.4: Configuration 1 for validating threshold values for the balanced High loading level.....	67
Figure A.5: Configuration 2 for validating threshold values for the balanced High loading level.....	68
Figure A.6: Configuration 3 for validating threshold values for the balanced High loading level.....	68
Figure A.7: Configuration 4 for validating threshold values for the balanced High loading level.....	69

Figure A.8: Configuration 5 for validating threshold values for the balanced High loading level.....	69
Figure A.9: Configuration 1 for selecting threshold values for the unbalanced High, Medium and Low loading levels.....	70
Figure A.10: Configuration 2 for selecting threshold values for the unbalanced High, Medium and Low loading levels.....	70
Figure A.11: Configuration 3 for selecting threshold values for the unbalanced High, Medium and Low loading levels.....	71
Figure A.12: Configuration 4 for selecting threshold values for the unbalanced High, Medium and Low loading levels.....	71
Figure A.13: Configuration 5 for selecting threshold values for the unbalanced High, Medium and Low loading levels.....	72
Figure A.14: Configuration 6 for selecting threshold values for the unbalanced High, Medium and Low loading levels.....	72
Figure A.15: Configuration 1 for validating threshold values for the unbalanced High, Medium and Low loading levels.....	73
Figure A.16: Configuration 2 for validating threshold values for the unbalanced High, Medium and Low loading levels.....	74
Figure A.17: Configuration 3 for validating threshold values for the unbalanced High, Medium and Low loading levels.....	74
Figure A.18: Configuration 4 for validating threshold values for the unbalanced High, Medium and Low loading levels.....	75

Figure A.19: Configuration 5 for validating threshold values for the unbalanced High, Medium and Low loading levels.....	75
Figure A.20: Configuration 6 for validating threshold values for the unbalanced High, Medium and Low loading levels.....	75
Figure A.21: Configuration 7 for validating threshold values for the unbalanced High, Medium and Low loading levels.....	76
Figure B.1: Step 1 of the wavelet-based fault detection and identification algorithm: data acquisition and preprocessing	77
Figure B.2: Step 2 of the wavelet-based fault detection and identification algorithm: fault detection, identification and display of the voltage waveform and wavelet coefficients.	78
Figure B.3: Step 3 of the wavelet-based fault detection and identification algorithm: grounding determination and output of fault information to the user.....	79

ABSTRACT

A Hardware/Software Platform for Fault Detection and Identification in Electric Power Distribution Systems for Testing Various Detection Schemes

Christian M. Schegan
Dr. Karen N. Miu, Ph.D.

Distribution systems are seeing a larger penetration of intelligent devices such as digital protection devices, advanced metering equipment and distributed generation. These devices are generally equipped with processors, which are capable of advanced computations. With advanced measurement and computation, faster and improved fault detection and identification techniques can be investigated.

Since actual fault data is rarely released for testing such techniques, research relies heavily on data collected from a simulation tool. This thesis proposes a hardware/software platform for performing fault experimentation in Drexel's Reconfigurable Distribution Automation and Control (RDAC) laboratory. Specifically, hardware setups have been designed to test a software implementation of a wavelet-based fault detector. This approach to fault studies preserves uncertainty stemming from system parameters and equipment. The effects of load on fault detection are studied with single-, two- and three-phase resistive and series resistive/inductive loads. While a wavelet-based approach was taken in this work, the hardware platform can be used with any detection scheme.

The discrete wavelet transform has been recently implemented for power quality analysis and fault detection. For fault detection, most work focuses on balanced power systems using per phase analysis. This thesis proposes a wavelet-based fault detection and identification algorithm capable of detecting and identifying faults within $\frac{1}{4}$ cycle of

a 60Hz signal in unbalanced radial distribution systems. Fault experiments under a wide range of load distributions and loading levels have been performed in order to design and validate the algorithm's performance. In addition, studies have been performed on meter placement, sensitivity and detection error with respect to various fault types and locations, in order to further increase the algorithm's reliability.

CHAPTER 1: Introduction

Electrical power distribution systems are responsible for supplying power to dispersed residential, commercial and small industrial customers in a safe, reliable and economical fashion. This is achieved by maintaining a reliable voltage level, correcting the power factor through use of reactive compensation and offering as close to continuous service as possible in order to meet demand. Service interruptions, although sometimes planned for, are to be minimized. However, it is the unplanned outage events, which are the focus of this thesis.

Distribution system faults are most commonly single or double phase faults. These faults occur when one or more phases come in contact with one another, the ground, or in some case both and can lead to temporary or permanent service outages. Many types of events including lightning flashover, animals, tree limbs and poor weather conditions, such as ice, high winds, and rain, are common causes of these service outages. Depending on whether any conductors, towers, or other parts of the infrastructure are damaged during such an event will determine whether a fault will cause a temporary or permanent service outage. It is therefore advantageous to detect and identify fault events as quickly as possible so that proper measures can be taken to restore service back to normal operating conditions.

1.1 Motivation

Fault detection and identification is of special interest to the electric utility industry and customers alike. The occurrence of a fault can prove to be extremely detrimental to the power system infrastructure as well as to the service reliability if improperly

diagnosed. With the increased penetration of intelligent devices equipped with Central Processing Units (CPUs) and the capability to measure, compute [1, 2] and communicate with other devices extra emphasis has been placed on research in the field of Fault Detection, Isolation and Recovery (FDIR) [3-9].

In the past, several approaches have been pursued including, but not limited to, the Discrete Fourier Transform (DFT), the Short Time Fourier Transform (STFT) [10, 11], the Discrete Wavelet Transform (DWT) [4, 5, 7, 11-17] and Artificial Neural Networks (ANNs) [8]. In this thesis, the selected method of fault detection and identification was the DWT for illustration.

Since, actual fault data is rarely available, in the past data to test fault detection algorithms were often generated from simulations. In addition, the system loads are frequently removed or simplified during fault studies because of the relatively large size of fault currents with respect to the load currents. Therefore, the power systems simulated are generally reduced from a large system with many buses and loads to a much smaller system [5, 7, 8]. These small-scale systems often consist of a generator at the sending end of a transmission line and a load at the receiving end. While testing on simulated, reduced systems demonstrated positive results. This thesis attempts to address some of the assumptions made in previous works.

A hardware/software platform will not require system simplification. Thus loads and load distributions impacts on fault detection and identification can be studied. In addition, the concept and effects of measurement location with respect to fault detection and identification can be studied because network structure will be preserved.

1.2 Background

The detection of faults has been the interest to power utilities and research for many years. However, fault data is difficult to obtain due to the statistically low occurrence of system faults. Texas A&M University has been particularly interested in the study of high impedance fault in electric power distribution systems and therefore has designed a test bed for high impedance faults at their Downed Conductor Test Facility [18-20]. Electric Power Research Institute (EPRI)-member utilities have also cooperated by installing distributed measurement devices on 60 feeders across North America [21]. This data monitors everyday system activity that can be used for the analysis of aging system components, disturbances and incipient fault conditions. By staging faults in distribution systems, in conjunction with utilizing the everyday system data, actual data can be made available for fault analysis.

Transient analysis has been addressed by certain techniques such as the STFT and DWT. Relevant details of the STFT and DWT will be presented in the following chapter. A summary of select literature is now discussed.

The STFT is similar to the traditional DFT multiplied by a window of fixed length. By translating this window across the desired signal and multiplying it with the DFT it is possible to localize transient behavior in both time and frequency, provided that an appropriate window length is chosen.

The DWT is a transformation in which the window is a function of finite duration and constant area that decays quickly to zero. This function is capable of being dilated or compressed as well as translated across the desired signal. One important property of the window function is that it maintains constant area when dilated or compressed.

Consequentially a superposition of these dilations and translations results in the ability to perfectly reconstruct the original signal, without aliasing and the need to choose an appropriate window length. This also allows for better localization of transients time and frequency.

Disadvantages to using the DWT include errors or difficulties analyzing certain types of signals if a mother wavelet is chosen that is not well suited for the particular purpose at hand. The problem with choosing a proper mother wavelet is similar to selecting an appropriate window size when using the STFT. The advantage however is that only one mother wavelet needs to be chosen for all frequencies, whereas the STFT requires several different window sizes for the same ranges in frequency. The output of the DWT results in coefficients that correspond to the detail of the signal at a particular frequency. Selecting threshold values to filter the important detail coefficients can be a difficult process, but it also necessary for the STFT.

The STFT and DWT have been applied in the analysis of voltage disturbances to allow for better localization in time and frequency. It was shown in [10] that the STFT performed better than the DWT for harmonic analysis because it is better suited to identify periodic or stationary behavior. However, the DWT, using a Daubechies-4 wavelet (db4), performed better at identifying the start and end of a disturbance [10]. The Daubechies wavelet is very well suited for identifying short-time, high frequency transients, as well as low frequency behavior over longer periods of time. In both cases the signals are non-periodic or non-stationary [17]. This behavior is appropriate for fault detection and shall be exploited in this thesis.

In [12-14, 16] it is shown that the Discrete Wavelet Transform (DWT) is an accurate and viable way to detect and analyze certain power quality problems. Since the DWT inherently possesses the ability to localize a signal well in both time and frequency, multiresolution analysis (MRA) can be performed, thus outperforming the traditional Discrete Fourier Transform (DFT)[22].

More recently research has moved towards using either STFT or DWT for fault detection, identification and location in balanced power systems. It appears that the DWT is still favored to the STFT for fault detection and identification due to its ability to automatically adjust the window size or scale the mother wavelet. One instance however where the STFT performed better than the DWT was during the location of line-to-ground faults [5]. These simulations were performed using current waveform data obtained from the Matlab's SimPowerSystem package. Another advantage of the DWT is that it reduces redundancy of coefficients by discarding half of the samples at each level, which correspond to the smoothed, less detailed part of the signal [10]. So long as an orthonormal wavelet such as the favored Daubechies wavelet is chosen, perfect or near-perfect signal reconstruction is possible [23].

The DWT using the db4 wavelet was also implemented in [24] for a fault location algorithm. This algorithm used travelling wave theory in transmission lines to locate where the fault had occurred. The voltage waveforms were separated into their respective decoupled modal components by Clark's Transformation and then analyzed using the DWT. The algorithm was independent of the fault impedance and was insensitive to mutual coupling between lines, as well as series compensated lines. This approach used two separate levels of detail when determining whether the fault was grounded and

performed well when measurements were available at a single end or at both sides of the transmission line.

In [8] a three bus transmission network was tested using DWT with a db4 wavelet to decompose the signal, and train a Probabilistic Neural Network (PNN) for decision making. This network contained a loop, which is avoided in radial distribution networks, and contained a single 500MVA load at a power factor of 0.8. The results showed that when the DWT was used to train the PNN, faults were detected at a accuracy higher than 99%.

Another approach used in [7] aimed to detect and identify faults in EHV transmission networks through the use of several threshold values. This was performed on a two bus, 150km transmission line model with a generator at one end and a load at the other. This proposed algorithm makes use of the 4th and 9th detail coefficients to identify the fault and determine the threshold values. The 4th level details contain the non-harmonic and non-fundamental frequencies created by the fault, whereas the 9th level details contained most of the harmonic frequencies.

1.3 Problem Statement

Since the majority of works utilize simulated data or smaller sets of actual data where network conditions may or may not have been known, this work seeks to address this potential shortcoming by the development of a hardware/software platform. In addition, since state-of-the-art fault detection techniques utilize thresholding from a single measurement point (substation), this work seeks to investigate the impacts of meter locations on fault detection techniques in multiphase distribution power systems.

1.4 Organization of Thesis

The flow of the thesis is now described. Chapter 2 offers a brief review of several topics relevant to the thesis. These include fault analysis techniques using the short-time Fourier transform and the discrete wavelet transform, followed by loading models and load types used in fault analysis and finally, meter location and sensitivity with respect to fault type and location. Chapter 3 then presents a statement of the problems to be solved. These include designing the hardware and software platforms, as well as choosing load types, loading levels and selecting meter locations for reliable fault detection and identification. Then, Chapter 4 discusses the solution methodology applied to the problems formulated in the previous chapter. Chapter 5 then presents the overall results of the wavelet detector's performance and specific hardware and software setups. Finally, Chapter 6 provides final conclusions on the work and details the contributions to the field of research. It also provides suggestions for future work.

CHAPTER 2: Review of Fault Analysis Techniques

The purpose of this chapter is to give a brief review of the concepts that are relevant to this thesis. Literature that has special importance to these topics is also discussed in finer detail than in Section 1.3. The chapter begins by briefly reviewing basic fault analysis concepts before discussing a select number of related techniques. The Short-Time Fourier Transform offers basic concepts needed to smoothly transition into explaining the discrete wavelet transform, which is utilized in this thesis. The next topic discusses common loading models and load types used in fault analysis and concludes with a brief review of meter placement and sensitivity.

2.1 Review of Fault Analysis

Distribution systems commonly consist of 1Φ , 2Φ and 3Φ lines, serving different types of dispersed customer loads. Faults occur when one or more phases of a distribution line come in contact with ground, another phase or object. Typically these events are due to animals, lightning, tree limbs, poor weather conditions, automobile accidents, etc. shorting or grounding one or more phases. These contingencies are unsafe to the public and often can damage conductors, insulators, or support structures and can result in extended loss of service for customers. For these reasons it is of utmost importance to detect the occurrence of all system faults, as well as which phase(s) are affected, as quickly as possible in order to clear the faults.

The line faults covered in this thesis are classified as follows:

- Line-to-Ground (LG)
- Line-to-Line (LL)
- Line-to-Line-Ground (LLG)
- Three-Phase (3P)
- Three-Phase-to-Ground (3PG)

At the inception of each type of fault, voltage and current transients are experienced by the distribution system. The relative magnitude of the transients depends on the number of phases involved and whether the fault is grounded. Figure 2.1 shows a circuit representation of a LL fault on phases A and B. The fault currents are indicated per phase by the notation I_{fa} , I_{fb} , and I_{fc} respectively. The fault impedance is indicated by Z_f and is dependent on certain conditions such as moisture in the ground, tower footings, tree limb, etc. Once a phase has been chosen as a reference, Phase A in this case, the resulting fault current is:

$$I_f = I_{fa} - Z_f I_{fb} \quad (0.1)$$

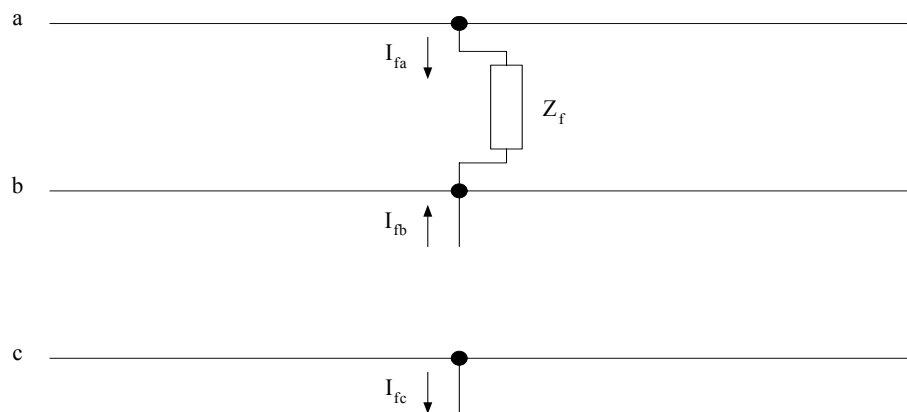


Figure 2.1: Three-phase circuit diagram of a Phase A-to-B, LL fault. The fault current for phases a, b, and c are I_{fa} , I_{fb} , and I_{fc} respectively. Z_f is the fault impedance.

Figure 2.2 shows the circuit diagram of a Phase-A-to-B-to-Ground fault. In this case the resulting fault current is the summation of both phases through the impedance Z_f .

$$I_f = (I_{fa} + I_{fb})Z_f \quad (0.2)$$

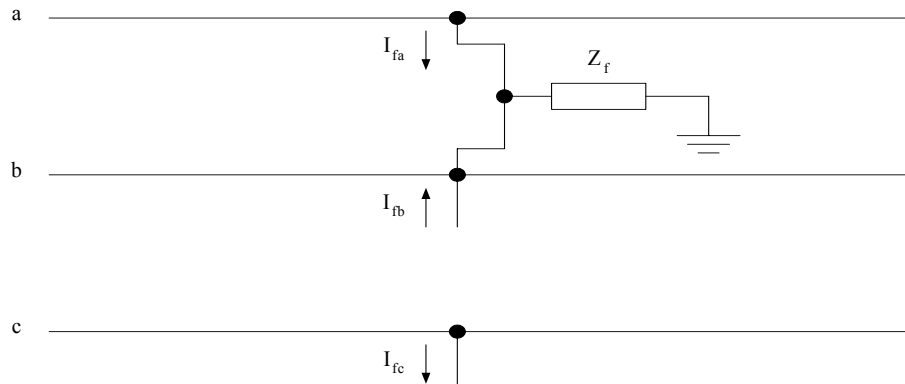


Figure 2.2: Three-phase circuit diagram of a Phase A-to-B-to-Ground, LLG fault. The fault current for phases a, b, and c are I_{fa} , I_{fb} , and I_{fc} respectively. Z_f is the fault impedance.

Therefore, a larger fault current is expected between grounded and ungrounded faults; whereas the unaffected phases should remain similar to before inception. These above mentioned relationships allow circuit breakers and protection equipment to detect that a contingency has occurred and allow them to open the respective phases.

2.1.1 Fault Detection Using the Discrete Short Time Fourier Transform

The Discrete Fourier Transform (DFT) has been traditionally used to analyze the frequency spectrum of periodic, stationary signals. This allows for localization in frequency but very poor localization in time [23]. When applied to non-stationary signals the DFT is therefore able to identify the frequencies that are present in a particular signal,

but has difficulty determining when they had occurred. In order to improve time-frequency localization the Discrete Short-Time Fourier Transform (STFT) was developed. The STFT differs from the DFT by multiplying the original signal by a Hamming window, essentially a bandpass filter, of fixed length and translating it over the length of the sampled signal (0.3).

$$X_n(e^{j\omega_k m}) = \sum_m x(m)w(n-m)e^{-j\omega_k m} \quad (0.3)$$

where:

$x(m)$: the signal to be analyzed,

$w(m)$: the window function of fixed length L

$\omega_k = \frac{2\pi k}{N}$: the frequency in radians with N frequency bands.

As long as $L \leq N$ perfect reconstruction is possible [10]. The size of the window function is directly related to the frequency range allowed to pass through the filter. A smaller window therefore has better frequency resolution by allowing high frequencies to pass through it; conversely, a larger window will have better resolution in time by allowing lower frequencies to pass through. If several frequency ranges are of interest, the STFT must be run with each of the corresponding window sizes.

In [10], the STFT was shown to accurately detect transient behavior and harmonics in power quality problems as long a reasonably small window size was chosen to allow the associated high frequency components to pass through the bandpass filter. The STFT was also used in [5] for fault identification and location on a power system consisting of a

generator and transformer at the sending end, which is connected through a 300km transmission line to a 200MVA load at a 0.9 power factor lagging at the receiving end.

The proposed algorithm performed very well at locating LG faults, outperforming DWT utilizing the Daubechies-4 mother wavelet, but did not perform as well the DWT at locating LL faults. Both algorithms, however, were able to detect the fault and identify the affected phases with virtually equal accuracy.

2.1.2 Wavelet Transform, Filter Banks and Their Application to Fault Analysis

The wavelet transform offers an alternative approach to using the STFT for the analysis of short-time, high frequency transients. The transform is performed similarly to the STFT, except that the “windowing function” is variable in size. This windowing function, also known as a Mother Wavelet, must possess several criteria in order to be admissible. These include oscillatory or wave-like behavior, an average value of zero about the time axis (x-axis) and quick decay to zero [22]. The Mother Wavelet is then subject to a scaling/dilation function and is translated across the desired signal. Like the Fourier transform, the wavelet transform also has a parallel in discrete time (0.4) [17].

$$DWT(m, k) = \frac{1}{\sqrt{a_0^m}} \sum_n x(n) g\left(\frac{k - nb_0 a_0^m}{a_0^m}\right) \quad (0.4)$$

where:

$g(k)$: the Mother Wavelet,

a_0 : the scaling factor,

b_0 : the translational factor

Each dilation and translation of the Mother Wavelet is called a Daughter Wavelet, and produces an associated wavelet coefficient, whose sum allows for signal reconstruction. Larger scaling values correspond to larger window sizes, yielding better time resolution and utility in the analysis of low frequencies. Conversely, smaller scaling values correspond to smaller window sizes, yielding better frequency resolution and utility in the analysis of high frequencies. The resulting wavelet coefficients for each scale show how well the signal and wavelet match. This leads to another important consequence of the wavelet transform, Multi-Resolution Analysis (MRA).

By setting a_0 equal to 2, b_0 equal to 1 while substituting for n and k , the DWT appears as in (2.3) [17].

$$DWT(m, n) = \frac{1}{\sqrt{2^m}} \sum_k f(k) \psi \left[\frac{n - k2^m}{2^m} \right] \quad (0.5)$$

where:

$$\psi \left[\frac{n - k2^m}{2^m} \right]: \quad \text{the Mother Wavelet.}$$

The above equation can be compared to a Finite Impulse Response (FIR) filter used often in signal processing. It can therefore be constructed using a filter bank consisting of high- and lowpass filters whose outputs are odd-indexed, alternating reversed-versions of each other. These are more commonly termed quadrature mirror filters.

At each level the signal is passed through a high- and lowpass filter. The output of the highpass filter is directly related to the higher frequency components of the original signal. This output is then down-sampled by a factor of 2, thus reducing the number of

samples by half. The resulting “detail” coefficients represent the signal detail at a frequency related to the scale of the mother wavelet. Similarly the output of the lowpass filter results in a smoother, less detailed version of the signal directly related to the lower frequency components. This output is then down-sampled by a factor of 2 and used as the input for the next level of high- and lowpass filters [23]. The detail coefficients from successive highpass filters represent increasing signal detail, which is directly related to higher frequency components of the original signal. The output of successive lowpass filters continues to smoothen the original signal for use at the next level of filters. This procedure is possible, so long as sampled data remains to continue downsampling. For a graphical representation, see Figure 2.3.

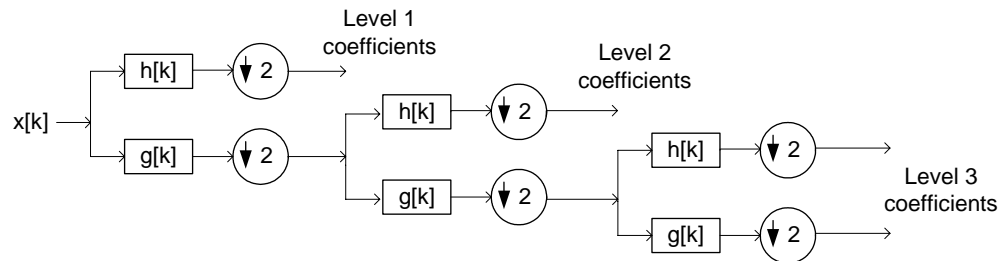


Figure 2.3: Filter bank representation of the DWT. Here $h[k]$ is a highpass filter, which yields the detail coefficients and $g[k]$ is a lowpass filter, which yields the course signal coefficients [23].

Down-sampling by a factor of 2 greatly reduces redundancy by effectively discarding half of the samples at each level with minimal to no loss of accuracy. This provides a computational advantage over the STFT and perfect or near perfect reconstruction is still possible by reversing the decomposition process and up-sampling by a factor of 2 at each level.

For applications to power system problems the authors of [7] developed a fault detection and identification algorithm for a 400kV EHV transmission line. The system consisted of a generator at the sending end, which is connected to a load at the receiving end through a 150km transmission line. The Daubechies-4 wavelet was chosen due to its computation speed and accuracy for both high and low frequency events. The algorithm checks the 4th level detail coefficient for three consecutive samples that exceed an initial threshold value. This signifies that a fault has occurred. The maximum absolute values of these coefficients are compared for all three phases. This determines which phases are affected by the fault. This process is then repeated for the ninth level coefficients in order to extract more detail with regard to the fundamental frequency. The ratios of the maximum absolute values per phase are then divided by the overall maximum of all three phases. The resulting values are then compared to four other threshold values, which classify the fault as LLL, LG, LL or an LLG fault. This algorithm experienced some problems distinguishing between LL and LLG faults due to an overlap in the range of the detail coefficient magnitudes. It also occasionally triggered a false alarm on an unaffected phase due to slight fluctuations caused by faults on the other phase(s). Overall the algorithm performed very well at detecting and identifying faults.

The DWT was also used in [8] to detect and identify faults on a three bus ringed transmission network. Each fault was created and simulated at various line lengths and inception angles in order to verify the algorithm's accuracy. All data was converted into their respective positive and negative sequence representation and the 1st level detail coefficients of the DWT were used to train and test a Probabilistic Neural Network

(PNN). By adjusting the spread of the radial basis layer to 0.002 it was possible to achieve accuracy of 99% while detecting the fault within $\frac{1}{4}$ of a cycle of a 60Hz signal.

2.2 Review of Loading Models and Load Types Used in Fault Analysis

Common loads in distribution systems are motor loads including condensers, refrigerators, AC units, etc. These loads contribute an inductive reactance to the system and therefore reduce the power factor. In addition, the loads are inherently unbalanced by nature. For instance one phase might service a residential area, while two or three phases generally service commercial areas. It is therefore advantageous to account for various types of loads such as R, RL and motor loads when testing a fault detection algorithm.

2.3 Review of Meter Placement, Measurement Sensitivity and Error

Distribution systems are predominantly radial networks or generally operated in a radial manner moving outwards from the substation. While substations inherently contain measurement equipment ongoing efforts involve placing measurement devices within the distribution network itself. It is therefore important to properly place accurate measurement equipment.

In [1] the measurement Jacobian was studied for an unbalanced radial distribution system. The first equation to be considered was the measurement equation (0.6).

$$z = h(V, \lambda) + v \quad (0.6)$$

where:

- $z \in \mathbb{R}^m$: the measurement vector,
- $h(V, \lambda)$: the real measurement function vector,
- $V \in \mathbb{R}^{3n}$: the bus voltage vector,
- $\lambda \in \mathbb{R}^{6n}$: the load parameter vector,
- $v \in \mathbb{R}^{6m}$: the random measurement error vector.

This equation represents the measured value of say voltage or current, which includes random error in addition to the actual value. Most measurement equipment is sold to be accurate within 3σ , or accurate 99% of the time. The measurement sensitivity of bus i with respect to the load at bus k is obtained by taking the partial derivative of $h_i(V, \lambda)$ with respect to λ_k by using the chain rule (0.7).

$$\frac{\partial h_i(V, \lambda)}{\partial \lambda_k} = \frac{\partial h_i(V, \lambda)}{\partial V} \frac{\partial V}{\partial S_{Lk}} \frac{\partial S_{Lk}}{\partial \lambda_k} = \gamma_k^i \frac{\partial S_{Lk}}{\partial \lambda_k} \quad (0.7)$$

where:

- $S_{Lk} \in \mathbb{C}^3$: the complex power of the load at bus k ,
- λ_k : the load parameter at bus k ,
- γ_k^i : the sensitivity of measurement i with respect to the load at bus k .

It was shown that as long as bus i and bus k are not on the same lateral or if $h_i(V, \lambda)$ is a voltage magnitude/phase measurement function then $\gamma_k^i \approx 0$. If however bus i and bus k

are on the same lateral or if $h_i(V, \lambda)$ is a power- or current flow measurement function then $\gamma_k^i \approx I$, where I is the Identity matrix. This means power- and current-flow residuals are highly dependent on load changes up- and downstream. When a fault is created, currents are injected into the system. Measurements are therefore sensitive to these current flows when the fault occurs on the same lateral and should be detected. When the measurement locations are on another lateral than where the fault had occurred, it is not expected to be detected. These two points will have an important role in this thesis and for the effectiveness of fault detection by different meters.

CHAPTER 3: Problem Formulation

In this chapter, first, a brief overview of the laboratory used to perform all of the fault experiments is presented. An overview of the existing hardware platform will be presented, followed by a discussion on the relevance of designing and adding an RL circuit equivalent motor load to the existing components. The third section begins by explaining the fault experiment's software and then highlights the original code for the wavelet detector. It ends by stating the algorithm's drawbacks and the proposed changes that were made. The fourth and fifth sections address the need for various load types, loading levels, proper meter placement and measurement sensitivity in order to maximize the algorithm's performance.

3.1 Problem Statement

The majority of works utilize simulated data [5-6,8-9] or smaller sets of actual data where network conditions may or may not have been known. In addition, several assumptions are generally made including:

- Since the ratio of fault currents are much larger than the load currents that are close to the fault location, loads can be aggregated to a fewer number of locations or even to a single location.
- It follows then that network structure can be simplified from many buses to a fewer number of buses [5-6,8-9], where a single phase analysis can be conducted for multiphase systems.

This work seeks to address the potential shortcoming of these assumptions by the development of a hardware/software platform. This platform would be able to collect actual fault data, allowing for various types of multiphase loads to be tested at several loading levels, while maintaining uncertainty from the system parameters and equipment, i.e. stochastic power and measurement hardware errors, slight variations in the impedance of system components, etc. These system components would be readily accessible and the experiments would be repeatable.

Due to the increasing number of distributed devices in distributions, which are capable of advanced measurements and computations, it is becoming possible for system disturbances to be detected simultaneously at locations other than a single measurement point (substation). Since current state-of-the-art fault detection techniques utilize thresholding from the substation, this work seeks to investigate the impacts of other meter locations on fault detection techniques in multiphase distribution power systems.

3.2 Hardware Platform for Experimentation

All hardware experimentation was conducted using Drexel's Reconfigurable Distribution Automation and Control (RDAC) laboratory [25]. The system shown in Figure 3.1 represents a 36-bus radial unbalanced distribution system with 4 feeder buses and 8 lateral feeders. The line segments of each lateral have the same impedances ratings, although due to slight differences in manufacturing, create a slight unbalance between phases. Four solid-state voltage relays act as normally closed switches and can be controlled remotely. Measurements are acquired from Hall-Effect Devices (HED) on three phases as well as the neutral wire and can be taken at any four buses at one time.

The measured signals are conditioned and then sent through an A/D converter in the Data Acquisition Card (DAQ) and outputted to the computer screen, creating a SCADA system. All laboratory modules, including the fault experiment used extensively in this thesis, have been custom designed for RDAC.

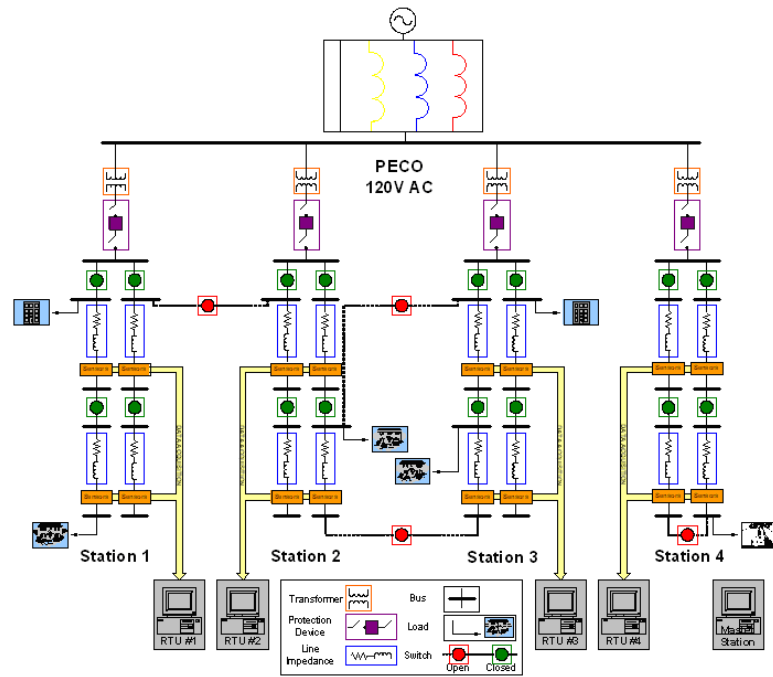


Figure 3.1 : One line diagram of RDAC laboratory setup including current limiting protection device [26].

The experimentation performed in this thesis is conducted on a single station within RDAC. A current limiting device was designed in [26] to protect the hardware in RDAC from being damaged by the rapid high current levels associated with system faults. This current limiting device was connected between the variable autotransformer and the distribution feeder box. The device utilized two 40mH inductors connected in parallel per phase and limited the current to 15A, approximately 5A below the maximum current rating of the system components. Another inductor box was also created in order to test

RL loads, which contained two 40mH inductors per phase that could be connected in series or parallel.

Since the purpose of RDAC is to perform hardware experiments relevant to the behavior of actual distribution systems, it is important to incorporate equipment for the study of steady state and dynamic conditions. Resistive and inductive components were previously available for diverse and easily interchangeable connections within RDAC. Incorporating motors loads into the fault experiments would further add to voltage and current dynamics during fault conditions and was therefore of special interest. Although, four 5-hp induction motors were available in the adjacent laboratory it was uncertain whether they could be safely connected because of their electrical characteristics. Therefore, before an actual induction motor could be connected to the system, an RL equivalent circuit model of an induction motor during steady-state operation was required to be proposed and tested.

The fault creating circuit designed for RDAC consists of six digital over-voltage relays shown schematically in Figure 3.2. The upper three relays are responsible for switching phases A, B and C to ground, whereas the lower three connect phases A to B, B to C and C to A respectively. Several relays can be used in unison to create 11 combinations of LG, LL, LLG and three-phase faults.

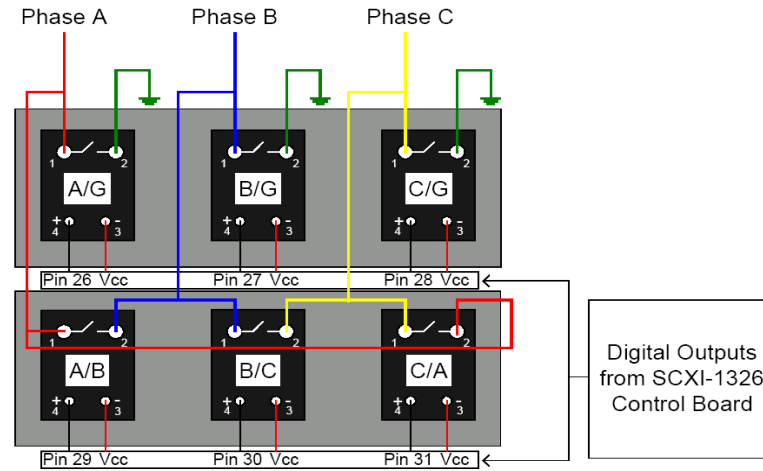


Figure 3.2: Over-voltage relays used for fault creation [26].

3.3 Software Platform for Experimentation

A Visual Basic Graphical User Interface (GUI) controls the fault experimentation laboratory in RDAC by allowing the user to first choose the bus that will be faulted and then the fault type (Figure 3.3). After a fault is created, the corresponding current and voltage waveforms are visible by clicking on the current limiting device on the main page. The current and voltage phasor data is available for all three phases and the neutral. This data includes measurements taken during the fault, as well as pre- and post-fault and is easily saved as a Microsoft Excel spreadsheet for post processing.

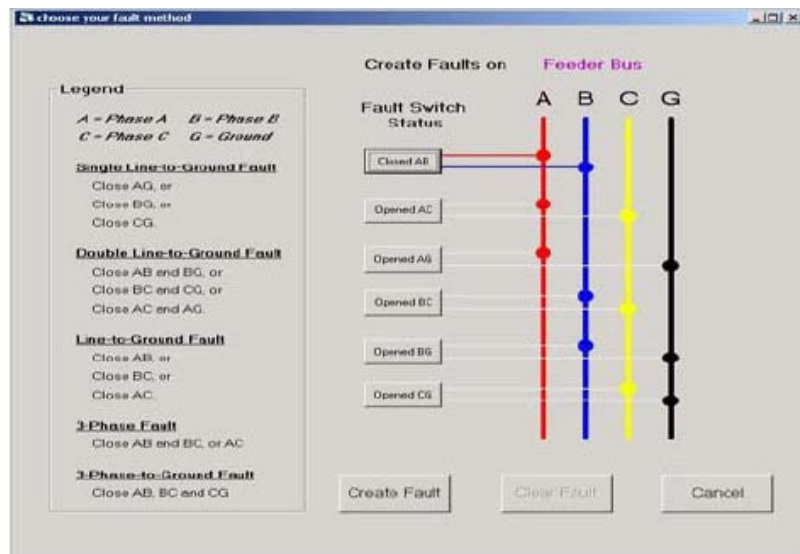


Figure 3.3: VBA GUI for fault creation [26].

Once the fault data has been collected any detection algorithm can be used to analyze it. The focus of this thesis is designing and testing a wavelet-based algorithm for fault detection and identification. The basic program was originally designed by [6] and uses the DWT to analyze the fault data. Since the inductor box limited the current, sometimes to an indiscernibly low level, it was decided to perform the DWT on the voltage waveforms. The user is able to see an animation of both the sampled signal and its second level wavelet coefficients for each phase. The detail coefficients are de-noised using a separate threshold per phase, such that only the coefficient corresponding to a fault will be analyzed.

Two drawbacks of the original code are its inability to distinguish between grounded and ungrounded faults and deliver a clear output to the user that states which phases were affected by the fault. At least one new threshold value would be required to decide whether a fault is grounded or ungrounded. The present output of the algorithm is the summation of numerical values assigned to each affected phase and can be confusing to

interpret. The new output will tell the user exactly what type of fault has occurred, whether it is grounded and display the approximate fault duration for the affected phases. Another addition to the code will prompt the user to enter the loading level of the system and apply the appropriate threshold values during the DWT analysis. These changes would allow for the algorithm to perform more reliably to changing load and also give a concrete output of the results.

3.4 Load Types and Loading Levels

The wavelet detector should reliably detect and identify faults for a wide range of load types and loading levels. The initial per phase threshold values in [6] were determined using only R loads at several different loading levels. In order for the experimentation to be truly representative of a distribution system, a variety of load types and connection types need to be chosen. The use of 3 Φ Wye-connected R and RL loads, as well as 1 Φ and 2 Φ R loads, ensures that the system's unbalanced nature is preserved. The effects of RL loads on the threshold values are of special interest, while several loading levels will also be examined to verify the detector's robustness.

It is important to maintain an approximately balanced voltage level for all three phases at the feeder bus, similar to the way actual distribution systems are planned. This voltage level must be attainable for all load levels and configurations. As a consequence, each loading distribution needs to be planned so that the phase-to-neutral voltages at the feeder bus are approximately balanced. Due to actual output limitations on the variable autotransformer under its highest loading level, this voltage level will be lower than the rated voltage value of 120V.

3.5 Meter Placement and Measurement Sensitivity

The next topic of interest is in the area of meter placement and sensitivity for successfully detecting that a fault has occurred. RDAC allows four measurement locations to be chosen while performing the fault experiment. The feeder bus is a natural choice for the first measurement location since it is directly connected to the substation. This measurement should be present in every test setup in hopes that it would accurately detect a fault and protect the substation. The other three measurements should be located both on the same lateral as the fault and also on the unaffected lateral, as to assess the sensitivity of the measurement location with respect to the fault. Another interesting point would be to observe the sensitivity of the measurement locations to the various types of faults and the physical locations of the loads. By retaining the system's structure it could aid in determining whether the network and load simplifications in previous works are valid assumptions for determining a detection algorithm's performance.

CHAPTER 4: Solution Methodology

This chapter details the steps taken in solving the hardware and software problems formulated in the previous chapter. The first section discusses topics relevant to the hardware experiment design approach. The second section discusses all topics relevant to the software design approach of the wavelet detector. These include the methodology utilized to select threshold values, choose appropriate load distributions, determine measurement sensitivity and finally highlight and explain all coding modifications and additions to the previously existing wavelet detector.

4.1 Experiment Design Approach

Section 4.1.1 gives an in-depth description of the methodology used to design an RL equivalent motor load from existing components available in RDAC. The next subsection discusses the need for varying loading levels and why certain load distributions were chosen. The final section presents the reasoning behind the choice of meter location and highlights several measurement schemes.

4.1.1 Designing an RL Equivalent Motor Load

The load types currently available for experimentation in RDAC include R and RL loads, both of which are passive elements. It is of strong interest to however to integrate a motor load in order to observe the voltage and current dynamics during system faults. Before an actual induction motor can be connected to the laboratory setup, an RL equivalent needed to be designed to model steady-state operation.

One RDAC inductor cart was available for use in the design of the motor load. The individual inductors were tested rigorously in [26] at various current levels. In order to choose the proper inductor cart for the motor load, a per-phase value of current magnitude was required at a desired rating of 208V and 4-hp (4.1). The value 745.7 is the conversion factor between W and hp.

$$|I| = \frac{P_{motor}(745.7)}{\sqrt{3}V_{LL}pf} = \frac{4(745.7)}{\sqrt{3}(208)(0.85)} = 9.7404A \quad (4.1)$$

where:

P_{motor} : real power rating of the motor in hp,

V_{LL} : line-to-line voltage,

pf : desired power factor.

In order to determine the required resistance and inductance values, it was then necessary to calculate the values of real power (P) (4.2) and reactive power (Q) (4.3) in kW and kVar respectively.

$$P = P_{motor}(745.7) = 2.983kW \quad (4.2)$$

$$Q = P \tan \theta = (2.983) \tan(31.788^\circ) = 1.849kVar \quad (4.3)$$

where:

$\theta = \cos^{-1}(pf)$: power factor angle.

With these values of P and Q the equivalent resistive (4.4) and reactive (4.5) components were calculated, as well as their ratio (4.6). Finally the equivalent inductance was determined from the reactance (4.7).

$$R = \frac{P}{|I|^2} = 31.439\Omega \quad (4.4)$$

$$X = \frac{Q}{|I|^2} = 19.483\Omega \quad (4.5)$$

$$\frac{X}{R} = 0.6197 \quad (4.6)$$

$$L_{calc} = \frac{X}{\omega} = \frac{19.843}{2\pi(60)} = 51.681mH \quad (4.7)$$

The inductance in (4.7) was then compared to the inductor data collected in [26]. The inductors whose values most closely matched this inductance were L_4 , L_{11} , L_{12} with inductances of 51.860, 51.813 and 51.310mH respectively. These values were linearly interpolated from the data for the current value determined in (4.1). An example calculation for L_4 is shown in (4.8) and used throughout the rest of the section.

$$X_{L_4} = \omega L_4 = (377)(0.0519) = 19.55\Omega \quad (4.8)$$

From (4.6) and (4.8), the effective resistance can be calculated (4.9).

$$R = X_{L_4} \left(\frac{R}{X} \right) - 1 = 30.547\Omega \quad (4.9)$$

Each resistive bank is composed of five 200Ω light bulbs per phase connected in parallel. Each light bulb is independent of the others and activated by a physical switch. The closest value of resistance to that in (4.9) is achieved through the use of five bulbs in parallel, yielding (4.10).

$$R_{eq} = \frac{R_{bulb}}{n_{bulb}} = \frac{200}{5} = 40\Omega \quad (4.10)$$

The larger resistance value consequently decreased the power factor angle and resulted in a power factor of 0.898 for the actual load.

4.1.2 Load Distribution for an Unbalanced Radial Distribution System

Distribution systems are inherently unbalanced; servicing dispersed 1Φ , 2Φ and 3Φ loads. Although this can lead to a slightly large imbalance at individual buses, systems are planned for and attempt to maintain a balanced overall load at the feeder bus. The load distributions used during experimentation were conducted such that a voltage of 110 ± 1 V was maintained at the feeder bus. Please see Figure 4.1 for a sample load distribution used for experimentation. This is composed of 1Φ , 2Φ and 3Φ R loads, as well as an RL equivalent motor load. All 2Φ and 3Φ loads were Wye-connected and grounded. The RL equivalent motor represents three single-phase induction motors in steady-state operation.

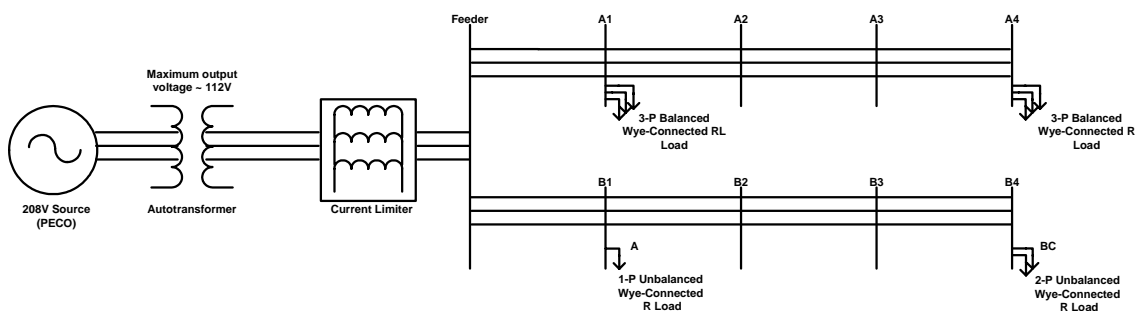


Figure 4.1: Schematic of a sample load distribution in RDAC, incorporating 1 Φ , 2 Φ and 3 Φ R loads, as well as a 3 Φ RL load.

In order to properly capture the effects of different loading configurations throughout the system on fault detection, 21 different load distributions were tested, varying fault and measurement locations. This involved moving different loads closer and farther away from the feeder bus, as well as changing the individual phases being serviced by 1 Φ and 2 Φ loads. One particular load distribution seen commonly in distribution systems is shown in Figure 4.2. One lateral was loaded with 1 Φ , 2 Φ and 3 Φ loads, simulating residential and commercial customers, while the other lateral was loaded to a much lesser degree using the RL equivalent induction motors. These RL loads symbolize an industrial customer, which is generally serviced on a separate feeder.

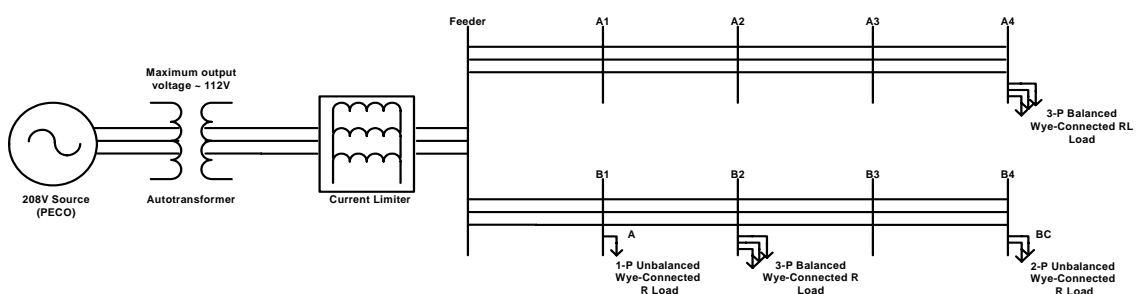


Figure 4.2: Schematic of a common load distribution where one lateral services an industrial client, while the other lateral services residential and commercial customers.

Since loading varies with the time of day and year, different loading levels were chosen. Three unbalanced loading levels were selected, namely High, Medium and Low, and corresponded to 5, 3 and 1 light bulb(s) respectively per phase. For each of these loading levels, the same load distributions, fault and measurement locations were tested. The results of approximately 2000 tests were used for selecting threshold values for Phase A, Phase B and Phase C.

Likewise, sets of completely different load distributions, totaling approximately 980 tests, were used to assess the performance of the wavelet detector utilizing the previously selected threshold values. These observations were used to test the impacts of previous assumptions for load and network simplification on testing fault detection schemes.

The High loading level was conducted again, this time on a balanced network utilizing strictly 3Φ R and RL loads. This case was conducted in order to observe the validity of the load and network simplifications on balanced power systems, particularly whether per phase analysis could be utilized for testing a fault detection and identification algorithm. For this situation approximately 2100 tests were performed for selecting threshold values for Phase A, Phase B and Phase C. A completely different set of approximately 1100 tests was used to assess the performance of the detector utilizing the predetermined threshold values.

4.1.3 Meter Placement

RDAC allows for meters to be placed at any bus. Meter placement was chosen primarily to observe the impacts of measurement locations subjected to various fault types and locations. Several measurement schemes were possible for certain load

distributions (Figure 4.3), where voltage and current measurements at any bus could always be used for fault detection and identification. Other possible configurations had only one or two reasonable choices (Figure 4.4). For example, meters could be placed at any bus in Figure 4.3; whereas a meter placed at buses B3 or B4 in Figure 4.4 would not offer any useful information, since the buses are unloaded and there are no downstream loads. Therefore discernable current would not be expected to flow past bus B2.

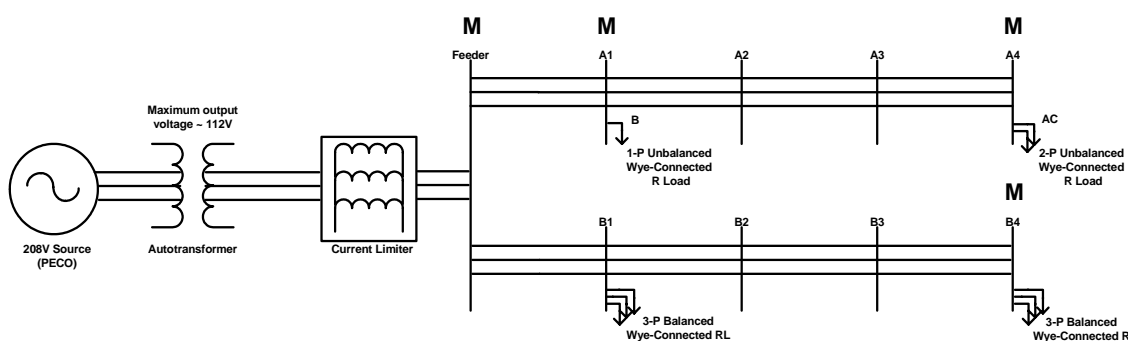


Figure 4.3: Sample load distribution where several measurement schemes are possible. Measurement locations are represented by an M above the respective bus.

Five different measurement locations were used throughout all load distributions and loading levels. These five locations included the feeder bus (F), Bus A1 (A1), Bus A4 (A4), Bus B1 (B1) and Bus B4 (B4). Although these measurement locations were chosen for this thesis, other locations can be chosen for future work. Because the substation is a critical bus in both transmission and distribution systems, F was selected or measured for all tests. The remaining three were placed on any buses that either had a load or a downstream load. This ensured that useful voltage and current information could be measured for fault detection and identification.

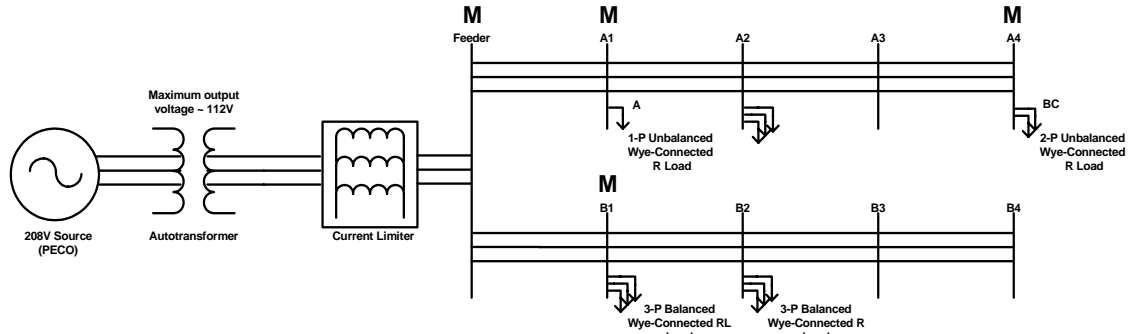


Figure 4.4: Sample load distribution where measurement schemes are limited.

From analytical properties of the Measurement Jacobian [1], it is expected for measurements located on a different feeder to be less sensitive than those located on the same feeder where the fault had occurred. In addition, all HEDs in RDAC have been specified to be accurate within 3σ and are independent and identically distributed; therefore, they do not affect each other when a measurement hardware error occurs. These factors were used in determining the impacts of meter location on fault detection and identification.

Multiple experiments were performed in which:

- load distributions,
- loading levels,
- fault locations and type,
- and meter locations,

were varied in order to diversify the fault data for post-processing. Post-processing was then conducted using a fault detection and identification algorithm. This particular algorithm used a wavelet-based approach for fault detection and identification.

4.2 Wavelet Based Fault Detector Algorithm

This section discusses the methodology used designing a wavelet-based software platform for fault detection and identification. Section 4.2.1 discusses how threshold values were selected for each phases A, B and C at several different loading levels. The next section discusses the advantages and consequences of testing a wide variety of load distributions on the robustness of the detector. Section 4.2.3 continues further by discussing the impacts of varying fault location and type on the sensitivity of measurement locations and how measurement equipment errors were distinguished from detector errors. The final section presents the three distinct portions of the detection algorithm; namely user input and preprocessing of data, fault detection and identification using the DWT and finally the output of results to the user. The modifications and additions to the previously existing code are highlighted accordingly.

4.2.1 Selecting Threshold Values

From Figure 4.4, it is shown that a current limiter was used to reduce large fault currents from damaging the hardware in RDAC. As a result, fault currents at certain locations were sometimes reduced to an indiscernibly low value. The wavelet-based algorithm therefore utilized voltage measurements for fault detection and identification.

The voltage signals were sampled at a rate of 3.6kHz, or effectively 60 times per cycle of a 60 Hz signal. The wavelet-based algorithm then analyzed this data using a window size of 256 data points at one time. The window size allowed for each set of data points to be decomposed into as many as 9 levels of detail. Before any analysis was conducted an appropriate mother wavelet needed to be chosen.

The wavelet chosen for this algorithm was the Daubechies-4 wavelet because it is very well suited for identifying short-time, high frequency transients, as well as low frequency behavior over longer periods of time, making it advantageous for fault detection and identification [10]. The second level detail coefficients of the voltage measurements were utilized by this algorithm due to the relatively tight grouping of well-defined coefficient magnitudes with respect to sample number. These characteristics are shown in the lower three plots of Figure 4.5.

Threshold values needed to be chosen in order to extract the detail coefficients corresponding to the inception of a fault. All other coefficients were not useful in detecting and identifying faults. These values were first selected by observing the minimum detail coefficient at fault inception for all types of faults, shown in Figure 4.5 by the circles on the lower three graphs. The threshold values were selected in this manner in an effort to minimize missed detections.

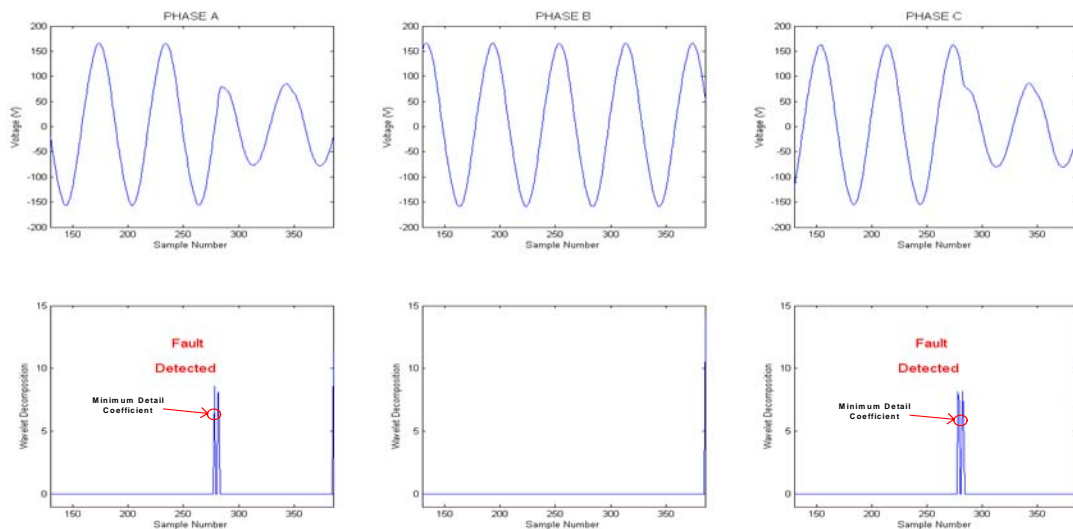


Figure 4.5: Output of the wavelet-based algorithm for a LL fault on phases A and C, showing the minimum detail coefficient at fault inception used for selecting threshold values.

Furthermore, each phase is sensed, at each measurement location. Thus a separate threshold was selected for each phase. Since the algorithm did not utilize measurements of the neutral, it did not require a threshold value.

The threshold values were then slightly adjusted in order to reduce the number of false alarms and also signal noise caused by distortion of the voltage waveform. This however, led to certain instances of missed detections. Figure 4.6 presents an example of this signal noise in order to clearly show what is meant by noise. The circles identify all points of distortion to the voltage waveform that resulted in unwanted spikes in the output of the wavelet-based algorithm. Physically these correspond to harmonics present in the power being supplied from the substation. The dotted lines show this voltage distortion and the corresponding wavelet detail coefficients. All other detail coefficients correspond to the LL fault on phases B and C.

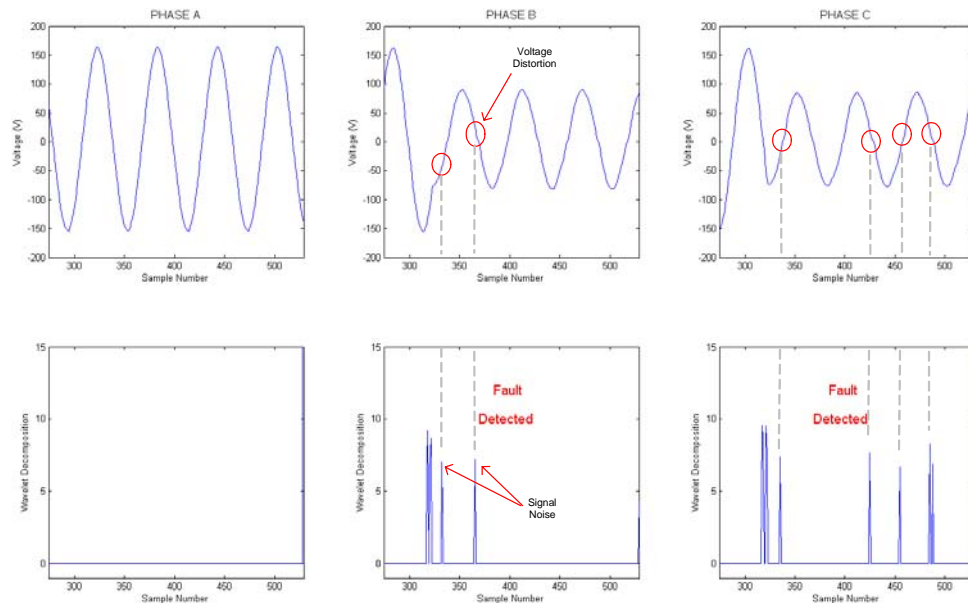


Figure 4.6: Output of the wavelet-based algorithm for a LL fault on phases B and C, showing a noisy output due to distortion of the voltage waveform.

The coefficients for LL and LLL faults were lower than those of other fault types. If for some reason a detail coefficient was much lower than normal it was assumed, and later verified, that either a physical meter error had occurred or that the meter was located at the end of another lateral.

By accepting this approach missed detections, as well as false alarms, were minimized. This was performed for all of the approximately 2100 tests conducted at each loading level. The hardware/software platform allowed for many different scenarios, i.e. load distributions, meter locations and fault locations to be tested, all while preserving uncertainty from the system parameter and equipment. This in turn allowed for the threshold values to be selected from a wide range of data, making the detector more robust to changing system events.

4.2.2 Load Distributions and Loading Levels

Distribution systems experience a variety of loading levels throughout the day. Loads can connect to, or disconnect from, the system causing fluctuations in load location and loading levels throughout the system. It is therefore important for a fault detector to perform the same when subjected to a wide variety of load distributions at varying loading levels. The hardware/software platform in RDAC allows for all of this data to be collected by physically connecting R and RL loads in 1Φ , 2Φ and 3Φ formations to any of the 9-buses. Each load can then be increased or decreased by physically switching a greater or fewer number of light bulbs on or off on a per phase basis. Schematics of the load distributions, as well as the number of light bulbs used for selecting thresholds and validating the algorithm's performance at each load level, are available in Appendix A.

4.2.3 Measurement Sensitivity

Another benefit of the hardware/software platform is that since the system's structure is preserved, studies on the impacts of meter location on fault detection and identification can be conducted. Meters can be placed at any four buses within the system at one time. It is of interest to see which meter locations can reliably detect and identify faults subjected to varying fault type and location.

Due to analytical properties of the Measurement Jacobian, we expect reliable detection on the same lateral where the fault was created. Therefore all missed detections and false alarms that occurred on the same lateral as the fault or at the feeder bus were recorded as detrimental to the detector's performance and were to be minimized. At the same time all missed detections and false alarms were recorded for measurements on the other lateral. These measurements were used to verify the expected results from the Measurement Jacobian and validate the performance of the detector.

In the event that a detection or identification error occurred on the same lateral as the fault, the experiment was repeated 5 times using the same configuration and respective loading level. In many, but not all cases, these errors would not occur again and were then termed as physical measurement hardware errors rather than detector errors.

An example of this methodology is presented in Figure 4.7, where a fault was created at bus B2. Meters located at F, B1 and B2 are expected to detect that a fault had occurred, whereas the meter at A4 would not be expected to detect the fault.

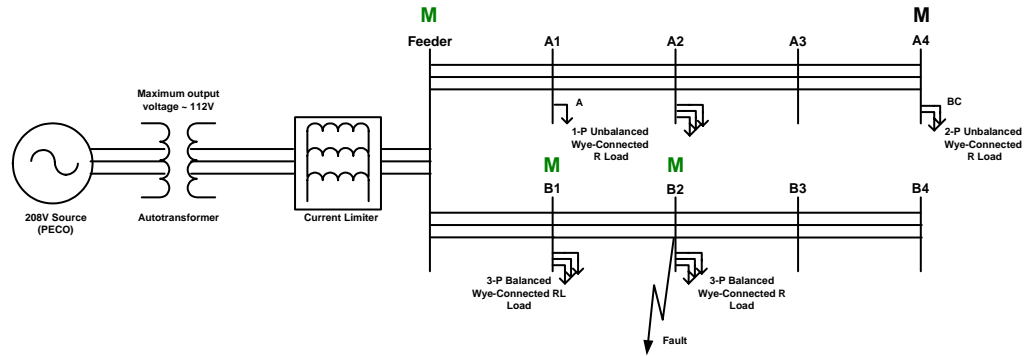


Figure 4.7: A sample load distribution with measurements at buses F, A4, B1 and B2. A fault occurred at bus B2.

In the event that one of the meters at F, B1 or B2 did not detect the fault, the experiment was performed another 5 times under the same conditions. If the error did not occur again, a measurement hardware error had occurred. These errors, however rather rare, were unable to be prevented.

4.2.4 Wavelets Detector Modifications and Coding

Initial code for the wavelet-based detector existed from [6]. The features include:

- Fault detection,
- Identifying which phases were affected,
- Approximate fault duration.

Some portions of the code, for example, the thresholding used for detection and identification, needed to be improved. These improvements would assign threshold values for various loading levels, as opposed to a single set of thresholds for all loading levels. Other features, for example, fault identification, needed to be expanded in order to

detect whether a fault was grounded or ungrounded. Finally, the output of the original code was designed to interface with a GUI coded in Visual Basic. This GUI was not available and the output needed to be presented clearly in the Matlab command window. This would reduce human error when analyzing the results which are now explained.

When identifying the affected phase, a numerical value was assigned to each affected phase, i.e. Phase A (1), Phase B (5) and Phase C (9). The summation of these values was then outputted to the user to identify the fault type. This however required the user to remember which values represented 7 different types of L, LL and LLL faults and did not identify whether the fault was grounded. In addition, the fault duration calculation assumed that the fault was cleared and did not necessarily use the sample number of the initial detail coefficient at fault inception. This often resulted in an erroneous calculation. The same threshold values were also used for several loading levels and were determined using only R loads, resulting in unnecessary missed detections and false alarms when other load types were used. Towards correcting these problems, modules were added, which prompted the user for the loading level, thus using the appropriate threshold values for fault analysis, and determined whether the fault was grounded. The remaining portion of this section describes how these problems were remediated and gives a brief description of the code that was written.

Threshold values were determined for three loading levels from a diverse set of load distributions, fault locations, fault types and meter locations. By prompting the user for High, Medium, or Low load levels, the appropriate threshold value could be used for analysis. This reduced the number of missed detections and false alarms as compared to using the same set of threshold values for all loading levels.

The fault duration calculation performed incorrectly when the start of a fault was improperly detected. If, for example, the clearing of the fault was detected but the start of the fault was not, the output of the fault duration calculation was the duration of the entire sampled signal. This was remediated by setting the fault duration equal to zero if the start of the fault was not detected. An output of zero clearly reported when a missed detection had occurred and eliminated negative fault duration values.

In some cases the first sample to exceed a threshold was not used for the calculation. This occurred because the fault start matrix (XFS) was not always arranged chronologically by the sample numbers at which they occurred. The X is used in this matrix as a dummy variable and represents the faulted phase, i.e. AFS denotes fault start on Phase A. This problem was corrected by first determining the index in XFS with the minimum sample number. The corresponding coefficient was then used for the calculation.

A threshold value was determined to decide whether a fault was grounded. The value chosen needed to distinguish between LL, LLL faults and their grounded counterparts. All grounded faults resulted in detail coefficient magnitudes that were much larger than when ungrounded. By selecting the minimum coefficient value of all LLLG faults as the threshold, the number of false identifications amongst LLL and LLLG faults were reduced. It was also a valid approach for distinguishing between LL and LLG faults, as the coefficients tended to be within the same range of values.

An easily interpretable output was desirable now that it was possible to identify all 11 types of faults under consideration in the RDAC. Grounded faults were also given a numerical value (11), similarly to the previous work in [6]. This was then added to the

summation of the affected phases. A series of if-then loops were written to correctly identify what type of fault had occurred. The output appeared in the command window stating what phases had been affected by the fault, whether it was grounded and gave and approximate fault duration for the affected phases. Flow charts of the entire fault detection algorithm are available in Appendix B. The areas that were modified or written for this thesis are also highlighted to distinguish them from the previous work.

CHAPTER 5: Experimental Results

This chapter shall show the effectiveness of RDAC and the designed hardware/software platform to create different scenarios with respect to fault detection. Previous works have often assumed that because fault currents are relatively large with respect to load currents located close to the fault location, loads can be aggregated from many locations to as few as one, therefore allowing for system structure to be simplified from many buses to generally fewer than three. The hardware/software platform presented in this thesis, however allows for various load distributions, loading levels, measurement locations, fault locations and fault types to be tested on a non-simplified, 9-bus, radial distribution network.

The first section presents the experimental procedure and methodology utilized when designing experimental hardware setups and collecting actual fault data. The following section presents the overall performance of the wavelet-based fault detector for each of the balanced and unbalanced loading levels, tabulating all missed detections, false alarms and false fault identifications, for each of the 11 fault types that were created. It also gives insight into particular load connections that contributed to these errors, as well as their relative location to the fault.

The third section demonstrates the need to consider several loading levels when designing a fault detector. Currently measurements are located at the substation with fewer instances of metering being dispersed throughout the system. Therefore, threshold values used for the high loading level were used by the detector for the data collected at the low loading level. The number of missed detections is then compared to the case where the low loading level threshold values are used for low loading level.

The final section discusses the impacts of meter location for detecting and identifying faults. It is then shown that the faults can be simultaneously sensed at locations within the system other than the substation, demonstrating the advantage of dispersing meters throughout the system.

5.1 Experimental Procedure

All hardware experiments conducted to select threshold values and validate the wavelet-based algorithm's performance were performed in the following manner:

1. A load distribution was designed such that a voltage of $110\pm 1V$ was maintained on all phases at the feeder bus and then physically connected in RDAC.
2. Measurement locations were chosen based upon system structure.
3. A fault location was chosen.
4. All 11 fault types were created at that location.
5. Steps 3-4 were repeated several times at different buses.
6. Steps 1-5 were repeated for several different load distributions.

While a wavelet-based detector was used in this particular case, this procedure can be used in conjunction with any detection algorithm. An example will now be presented, as to visualize the steps of this experimental procedure. This however is only one load distribution possible in RDAC.

The first step is to design a load distribution, for example the one pictured in Figure 5.1, such that the voltage of all three phase is $110\pm 1V$ at the feeder bus.

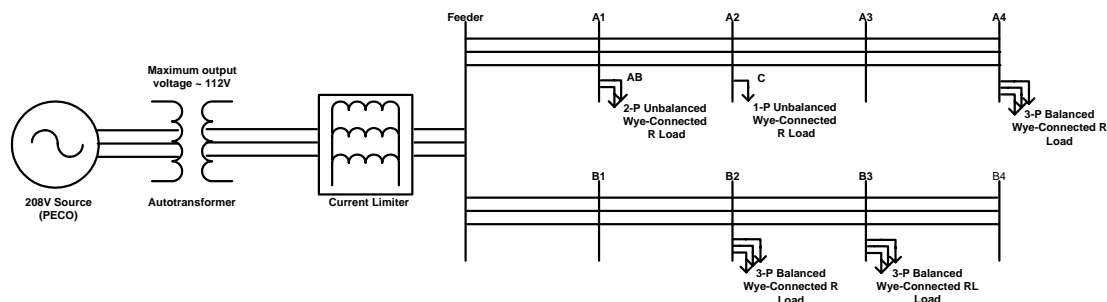


Figure 5.1: A sample load distribution used for experimentation.

For this particular load distribution, a number of possible meter locations exist. Bus B4 is the only location in this system that would not give any useful measurements. This is due to the absence of a load at Bus B4 and any downstream loads. The first measurement should be located at the feeder bus, since we expect measurement equipment at the substation, represented here by F. The remaining three measurements can be placed on any bus besides B4. The experiments conducted for this thesis utilized measurements at A1, A4, B1 and B4. An example of meter locations can be seen in Figure 5.2, represented by M.

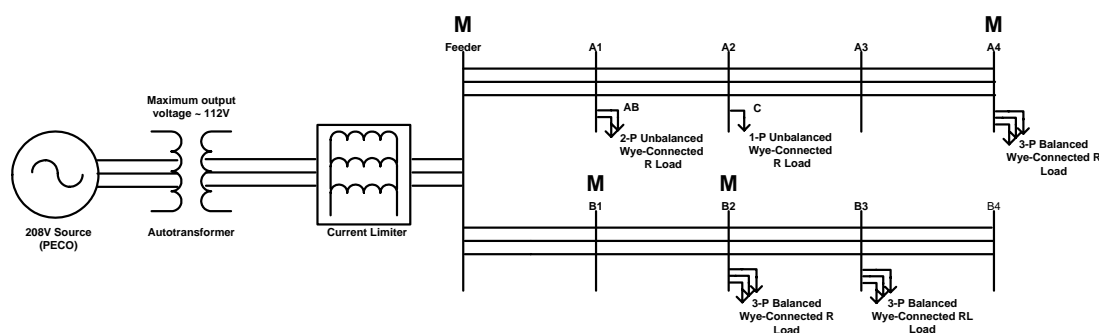


Figure 5.2: Measurements locations, represented by an M, are then chosen.

Now that meter location have been chosen, all 11 types of faults can be created at several fault locations. Figure 5.3 shows three of the seven possible fault locations at buses A1, B1 and B2. After all 11 fault types have been created at the selected fault locations, this procedure can be repeated with a new load distribution. All load and measurement distributions used in this thesis are illustrated in Appendix A.

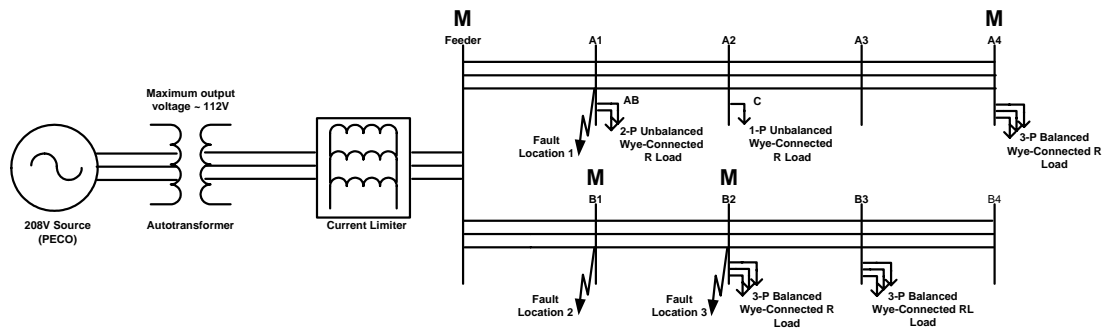


Figure 5.3: All 11 fault types are then created at each fault location. Here faults are located at buses A1, B1 and B2.

5.2 Overall Performance of the Wavelet Based Fault Detector

This section presents the overall performance of the wavelet based fault detector. Each subsection provides the threshold values determined for the corresponding loading level. In addition, the number of missed detections and false alarms are tabulated, as well as the overall accuracy of the algorithm for fault detection and ground identification.

5.2.1 Balanced High Loading Level

The threshold values in Table 5.1 were determined as a result of 2112 experiments using three load distributions, each with four measurement schemes. These experimental setups are shown graphically in Section A.1.

It is interesting to note that although all loads used for this loading level were balanced, the threshold values were not the same for each phase. This was due partially to slight deviations in line impedance, power hardware and measurement hardware. The significance of these values is that it shows that the assumption of using per phase analysis for testing detection and identification algorithms for balanced systems does not necessarily hold true. If for example the same threshold value was used for all three phases, unnecessary missed detection and false alarms would have been present.

Table 5.1: Threshold values for the balanced High loading level.

Threshold Values		
Phase A	Phase B	Phase C
5.1	5.35	5

After the threshold values were selected, approximately 1230 new tests were conducted to test the validity of the threshold values. These tests faulted previously unfaulted buses and tested five new load distributions, all of which are shown graphically in Section A.2. The results are tabulated in Table 5.2 and divided into missed detections, false alarms and detrimental errors, which occurred on the same feeder as the fault and were expected to be detected by analytical properties of the Measurement Jacobian. LG faults were detected 100% of the time and LLG faults experienced zero missed detections. Problems arose however in the case of LL faults, which experienced both

missed detections and false alarms. These particular instances, however few in number, suggest that a single set of thresholds is not sufficient for all fault types.

Table 5.2: Performance errors for the balanced High loading level.

Fault Type	Number of tests	Missed Detections	False Alarms	Detrimental Errors	Detector Accuracy (Raw Data)
AG	112	0	0	0	100.00%
BG	112	0	0	0	100.00%
CG	112	0	0	0	100.00%
AB	112	2	0	1	98.21%
BC	112	3	0	2	97.32%
AC	112	1	0	1	99.11%
ABG	112	0	1	0	99.11%
BCG	112	0	6	0	94.64%
ACG	112	0	7	0	93.75%
ABC	112	1	4	0	95.54%
ABCG	112	0	3	0	97.32%
Total	1232	7	21	4	97.73%

The overall accuracy of the fault detection algorithm for the balanced High loading level is presented in the last row of Table 5.2.

5.1.2 Unbalanced High Loading Level

The threshold values in Table 5.3 were selected from approximately 2000 experiments using six loading distributions. The experimental setups are available in Section A.3 and were used to select threshold values for all unbalanced loading levels. In

addition, 1 Φ , 2 Φ and 3 Φ Wye-connected R loads, as well as an RL equivalent motor load were connected and dispersed throughout the system for each load distribution. For this particular loading level, all three phases used the same threshold value. These values were relatively insensitive to change since the resulting detail coefficients of the DWT were much larger than at other loading levels.

Table 5.3: Threshold values for the unbalanced High loading level.

Threshold Values		
Phase A	Phase B	Phase C
6.5	6.5	6.5

The load distributions and measurement locations that were used for validation of the threshold values are available in Section A.4. The results again show that zero missed detections occurred for LG and LLG faults, however this time false alarms had occurred for both. The greatest impact on missed detections and false alarms was due to faulting buses with 2 Φ and 3 Φ connections. Particularly in the case of 2 Φ connections, unaffected phases showed a higher frequency of false alarms upstream from the fault location. This demonstrates the need to account for connection type, as well as load location when testing unbalanced radial power systems. The overall accuracy of the detector and fault identification algorithms are presented in the last row of Table 5.4.

Table 5.4: Performance errors for the unbalanced High loading level.

Fault Type	Number of tests	Missed Detections	False Alarms	Detrimental Errors	False Identification	Detector Accuracy (Raw Data)	Fault Identification Accuracy
AG	81	0	0	0	0	100.00%	100.00%
BG	81	0	4	2	0	95.06%	100.00%
CG	81	0	4	2	0	95.06%	100.00%
AB	81	2	2	0	0	95.06%	100.00%
BC	81	2	5	2	1	91.36%	98.77%
AC	81	0	3	2	1	96.30%	98.77%
ABG	81	0	2	0	5	97.53%	93.83%
BCG	81	0	3	2	3	96.30%	96.30%
ACG	81	0	2	0	0	97.53%	100.00%
ABC	81	1	2	2	2	96.30%	97.53%
ABCG	81	0	2	1	9	97.53%	88.89%
Total	891	5	29	13	21	96.18%	97.64%

5.1.3 Unbalanced Medium Loading Level

The threshold values in Table 5.5 were selected from the same number of load distributions and measurement locations as the unbalanced High loading level, except this time 3 parallel connected light bulbs were used per phase. The most sensitive phase for this loading level was Phase A, which required the largest threshold for reliable detection.

Table 5.5: Threshold values for the unbalanced Medium loading level.

Threshold Values		
Phase A	Phase B	Phase C
6.38	5.97	5.7

As seen for previous loading levels, missed detections occurred primarily amongst LL faults. This happened particularly when the fault location was at or near a bus with a 2Φ connection and measurements were upstream or on another lateral.

Table 5.6: Performance errors for the unbalanced Medium loading level.

Fault Type	Number of tests	Missed Detections	False Alarms	Detrimental Errors	False Identification	Detector Accuracy (Raw Data)	Fault Identification Accuracy
AG	81	0	3	1	0	96.30%	100.00%
BG	81	0	2	1	0	97.53%	100.00%
CG	81	0	2	1	0	97.53%	100.00%
AB	81	3	0	2	0	96.30%	100.00%
BC	81	2	1	2	0	96.30%	100.00%
AC	81	3	1	1	0	95.06%	100.00%
ABG	81	1	0	0	2	98.77%	97.53%
BCG	81	0	2	1	2	97.53%	97.53%
ACG	81	0	1	1	0	98.77%	100.00%
ABC	81	0	2	2	5	97.53%	93.83%
ABCG	81	0	0	0	2	100.00%	97.53%
Total	891	9	14	12	11	97.42%	98.77%

The overall accuracy of the detector and the fault identification algorithm are presented in the last row of Table 5.6.

5.1.4 Unbalanced Low Loading Level

The threshold values in Table 5.7 were selected as a result of testing approximately 2000 experiments using the same loading distributions, fault and measurements locations as the unbalanced High and Medium loading levels, this time using 1 light bulb per phase for each load. The most sensitive phase was Phase A, requiring the largest threshold for reliable detection, followed by Phase B. These values were still higher than those determined for the balanced High loading level.

Table 5.7: Threshold values for the unbalanced Low loading level.

Threshold Values		
Phase A	Phase B	Phase C
5.86	5.4	5

After the threshold values were selected, approximately 891 tests were conducted. These tests faulted previously un-faulted buses and tested new load distributions. As for previous loading levels missed detections for LG and LLG faults were minimal; however, for LL faults, the number of missed detections was much greater than the number of false alarms. These errors occurred primarily when buses with 2 Φ connections were faulted and were exacerbated further by the relatively low loading level in comparison to the size of the fault currents. This also suggests that need for separate threshold values for LL faults. The overall accuracy of the fault detector and identification algorithms is presented in the last row of Table 5.8.

Table 5.8: Performance errors for the unbalanced Low loading level.

Fault Type	Number of tests	Missed Detections	False Alarms	Detrimental Errors	False Identification	Detector Accuracy (Raw Data)	Fault Identification Accuracy
AG	81	0	1	0	0	98.77%	100.00%
BG	81	0	0	0	0	100.00%	100.00%
CG	81	0	0	0	0	100.00%	100.00%
AB	81	5	0	5	1	93.83%	98.77%
BC	81	10	0	6	1	87.65%	98.77%
AC	81	6	0	1	1	92.59%	98.77%
ABG	81	1	0	0	1	98.77%	98.77%
BCG	81	0	0	0	2	100.00%	97.53%
ACG	81	0	1	0	3	98.77%	96.30%
ABC	81	2	0	0	3	97.53%	96.30%
ABCG	81	0	0	0	3	100.00%	96.30%
Total	891	24	2	12	15	97.08%	98.32%

5.1.5 Comparison of Threshold and Detector Accuracy for Each Loading Level

This section focuses on:

- Limitations to simplifying load levels and
- The impact of 3 Φ systems during fault detection.

There are several points to notice about the threshold values in Table 5.9. The threshold values for the balanced High loading level were not the same for phases A, B and C. This can be due to factors such as power hardware error, measurement hardware, slight differences in manufacturing of hardware components, etc. If single phase analysis had been used to select the threshold values, assigning the same value to each phase, unnecessary missed detections and false alarms would have occurred. This case shows the need to consider all phases of the power system when designing a fault detection and identification algorithm, rather than performing a single phase analysis.

Table 5.9: Threshold values selected for all balanced and unbalanced loading levels.

Loading Level	Phase		
	A	B	C
Balanced High	5.1	5.35	5
Unbalanced High	6.5	6.5	6.5
Unbalanced Medium	6.38	5.97	5.7
Unbalanced Low	5.86	5.4	5

For the unbalanced High, Medium, and Low cases, it is important to notice that the threshold values per phase tend to decrease with decreasing loading level. If the same set of threshold values were used for all loading levels, missed detections or false alarms would occur more frequently as the loading level increased or decreased respectively. In

Table 5.10, the threshold values corresponding to the High loading level were used by the detector for measurements at the substation (F) at the Low loading level. The number of missed detections was approximately double the number when the threshold values for the low loading level were used. Bus F was chosen as the reference location, since measurements capabilities are currently present at the substation. The increased number of missed detections demonstrates the need for threshold values to vary with the level of load. A single set of threshold values would not be sufficient to handle a wide variety of loading levels and are necessary for a robust detection and identification algorithm.

Table 5.10: Threshold values for the High and Low loading level were used by the detector for the Low loading level. Measurements were taken at the substation (F).

Loading Level	Threshold Level	Missed Detections
Low	High	17
Low	Low	8

Table 5.11 presents the overall performance errors for all of the balanced and unbalanced loading levels. The number of missed detections was lower than the number of false alarms for all cases except the unbalanced low loading level. The discrepancy comes from the much larger ratio of fault currents to load currents, as well as a greater signal to noise ratio for measurements. The impacts of faulting buses with 2Φ loads contributed to missed detections and false alarms for all loading levels but had an even greater effect on the low loading level. This demonstrated that load connection, fault type and location, and load distribution affected the detection algorithm's performance,

therefore suggesting that system structure should not be simplified when designing an algorithm for fault detection and identification in radial unbalanced power systems.

Table 5.11: Overall performance errors for all balanced and unbalanced loading levels.

Loading Level	Missed Detections	False Alarms	Detrimental Errors	False Identification	Accuracy (All)	Fault Identification Accuracy
High (Balanced)	7	21	4	N/A	97.73%	N/A
High (Unbalanced)	5	29	13	21	96.18%	97.64%
Medium (Unbalanced)	9	14	12	11	97.42%	98.77%
Low (Unbalanced)	24	2	12	15	97.08%	98.32%

5.3 Impacts of Meter Location of Fault Detection and Identification

This section focuses on the platform's ability to demonstrate the impacts of meter location on fault detection and identification. Examples are given to encourage dispersed metering throughout power distribution systems, as well as noting stochastic measurement hardware errors that occurred during experimentation.

When a fault was created on one lateral, measurements located at the end of the opposite lateral were unreliable at sensing the faults, despite the loading level. In addition, measurements located at the first bus of the opposite lateral were only reliable when the fault had occurred close to feeder bus. These results were expected from analytical properties of the Measurement Jacobian [1]. In all measurements located on the same lateral as the fault, it was expected for the fault to be detected. The ability to sense fault conditions at several locations simultaneously is beneficial and increases the overall safety and redundancy of system protection.

For example, during the unbalanced loading level, there were four instances in which F did not detect that a fault had occurred downstream, whereas the measurement at A1 did successfully detect. This shows the benefit of dispersing meters throughout the distribution system, rather than simply taking measurements at the substation. Had there not been any meters downstream from the substation, the fault would have gone undetected, possibly causing both safety and reliability problems.

The vendors of the measurement equipment used in RDAC stated that measured values should be within 3σ of the actual value. This corresponds to an average measurement error of at most 1%. If the detection of a fault was expected at a particular bus, previously defined as detrimental to the detectors performance, the particular fault was repeated 5 times using the respective measurement location. All equipment used in RDAC is generally tested rigorously; however, detailed testing information of the HEDs used for measuring was not available. If a particular error had not occurred again after 5 tests, it was determined that a measurement hardware error had in fact occurred. This testing method was therefore capable of determining which missed detections and false alarms were due to measurement hardware errors and not to the fault detection algorithm itself.

The total number of measurements and errors for the balanced High, and the unbalanced High, Medium and Low loading levels are separated by measurement location and tabulated in Table 5.12-5.14 respectively. The percent error values are calculated based upon the data at each measurement location. These values however only correspond to gross measurement error at that particular bus, which resulted in missed detections and false alarms.

Table 5.12: Bus measurement hardware errors for the balanced High loading level.

Bus	A1	A4	B1	B4	F
Total Number of Measurements	264	198	231	231	308
Total Number of Errors	0	3	0	6	3
% Error	0.00%	1.52%	0.00%	2.60%	1.36%

Table 5.13: Bus measurement hardware errors for the unbalanced High loading level.

Bus	A1	A4	B1	B4	F
Total Number of Measurements	165	108	132	198	198
Total Number of Errors	0	1	0	15	0
% Error	0.00%	0.93%	0.00%	7.58%	0.00%

Table 5.14: Bus measurement hardware errors for the unbalanced Medium loading level.

Bus	A1	A4	B1	B4	F
Total Number of Measurements	165	108	132	198	198
Total Number of Errors	1	2	1	8	1
% Error	0.61%	1.85%	0.76%	4.04%	0.45%

Table 5.15: Bus measurement hardware errors for the unbalanced Low loading level.

Bus	A1	A4	B1	B4	F
Total Number of Measurements	165	108	132	198	198
Total Number of Errors	1	2	1	4	1
% Error	0.61%	1.85%	0.76%	2.02%	0.45%

The measurements located at buses A1, B1 and F performed well within 3σ of the actual measurement, whereas buses located at A4 and B4 erred much more frequently. Not only were measurement errors more common at these buses, but also appeared to increase with increasing loading conditions. These errors as well as power hardware errors are however not preventable.

CHAPTER 6: Conclusions

6.1 Conclusions

This thesis has presented a hardware and software platform for fault analysis and identification. The hardware/software platform utilizes distributed devices in a 9-bus, unbalanced radial distribution system to create 11 types of faults at any location within the system. Data is collected through actual experimentation and preserves uncertainty from system parameters and equipment. The system's structure is maintained throughout all tests, contrary to many previous works, which assume that network simplification is permissible due to the fault current being much larger than the load currents. The loads within the distribution system have also not been simplified, utilizing 1 Φ , 2 Φ and 3 Φ R loads, as well as an RL circuit equivalent motor load. This can help determine whether network simplification is in fact permissible when studying the performance of fault detectors.

A wavelet-based algorithm has been created to reliably detect and identify various fault types at different system locations within $\frac{1}{4}$ cycle of a 60Hz signal. Threshold values were determined per phase for each different loading condition. Existing code was expanded to detect if a fault was grounded or ungrounded and output the results to the user in an easily interpretable fashion. While the detection algorithm presented utilized the DWT, any detection method could be tested using the hardware/software platform.

The final focus of this thesis was on the impacts of meter location on fault detection and identification. The hardware/software platform allowed for four meter locations out of the 9 possible locations to be measure at one time. While a subset of these 9 locations was used throughout this thesis, any combination could be used for future work. This

study could not have been performed had the system been simplified. The approach and results from this proposed method were validated and presented for use in unbalanced radial power distribution systems.

6.2 Summary of Research Contributions

The work in this thesis presented a hardware and software platform for fault detection and identification, which could be used to test any detection algorithm. As an example, a wavelet-based algorithm capable of reliably detecting and identifying various fault types at several loading levels was also designed. Specifically, this thesis:

- Designed and implemented various experiments for studying faults in power distribution systems.
- Designed and tested a wavelet-based fault detection and identification algorithm using the hardware/software platform.
- Demonstrated the impacts of various loading levels, load distributions and measurement locations on fault detection performance.

Thus this thesis draws attention to the fact that previous assumptions for load and network simplifications do not hold in power distribution systems.

6.3 Future Work

The presented methods have been shown to reliably detect and identify faults in a non-simplified 9-bus, radial power distribution system. The hardware platform allows for a wide range of testing scenarios to better represent real life power distribution systems.

This versatility provides experimental data from hardware experimentation capable of being used with any fault detection scheme.

Incorporating motor loads within the RDAC fault experiment laboratory is of special interest. Motor loads would enhance the versatility of RDAC by exhibiting dynamic load behavior during fault conditions. An attempt was made to incorporate a ¼ hp motor within RDAC, but was unable to be connected in a stable manner. The voltage imbalance per phase, even when limited to a maximum deviation of $110 \pm 1V$, caused the motor to experience rocking. Therefore, future work is needed to correct this voltage imbalance for safe installation of motor loads.

Another area of interest is the study of switching events, such as series capacitors used for reactive compensation, and whether they would have an adverse effect on the overall performance of any fault detection algorithm. For example, the wavelet-based fault detector that was designed and tested in this thesis was demonstrated to be a reliable and robust tool for fault detection and identification in radial distribution systems, but was not tested during such switching events.

Incorporating a method for fault location is also highly recommended for future research. Although there was often an overlap in detail coefficients for LL and LLL faults, the performance of the ground detection algorithm could be improved by determining a separate threshold to distinguish between the two fault types.

BIBLIOGRAPHY

- [1] W. Jie and K. Nan Miu, "A zonal-load estimation method for unbalanced, radial distribution networks," *Power Delivery, IEEE Transactions on*, vol. 17, pp. 1106-1112, 2002.
- [2] W. Jie and M. Karen Nan, "Meter placement for load estimation in radial power distribution systems," in *Circuits and Systems, 2004. ISCAS '04. Proceedings of the 2004 International Symposium on*, 2004, pp. V-916-V-919 Vol.5.
- [3] Z. Jun, D. L. Lubkeman, and A. A. Girgis, "Automated fault location and diagnosis on electric power distribution feeders," *Power Delivery, IEEE Transactions on*, vol. 12, pp. 801-809, 1997.
- [4] H. Douglas, P. Pillay, and T. H. Ortmeier, "The application of wavelets to shipboard power system protection," in *Electric Ship Technologies Symposium, 2005 IEEE*, 2005, pp. 432-436.
- [5] D. Das, N. K. Singh, and A. K. Sinha, "A comparison of Fourier transform and wavelet transform methods for detection and classification of faults on transmission lines," in *Power India Conference, 2006 IEEE*, 2006, p. 7 pp.
- [6] M. B. Mainkar K., Robles K., Villanueva A., "Fault Detection in Power Systems Using Wavelet Transforms," Drexel University, Philadelphia 2006.
- [7] K. Gayathri, N. Kumarappan, and C. Devi, "An apt method for fault identification and classification on EHV lines using discrete wavelet transform," in *Power Engineering Conference, 2007. IPEC 2007. International*, 2007, pp. 217-222.
- [8] T. Patcharoen, A. Ngaopitakkul, and A. Kunakorn, "Identification of fault types for a three-bus transmission network using Discrete Wavelet Transform and probabilistic neural networks," in *Power Engineering Conference, 2007. IPEC 2007. International*, 2007, pp. 1137-1142.
- [9] A. Borghetti, M. Bosetti, M. Di Silvestro, C. A. Nucci, and M. Paolone, "Continuous-Wavelet Transform for Fault Location in Distribution Power Networks: Definition of Mother Wavelets Inferred From Fault Originated Transients," *Power Systems, IEEE Transactions on*, vol. 23, pp. 380-388, 2008.
- [10] Y. H. Gu and M. H. J. Bollen, "Time-frequency and time-scale domain analysis of voltage disturbances," *Power Delivery, IEEE Transactions on*, vol. 15, pp. 1279-1284, 2000.
- [11] S. Santoso, W. M. Grady, E. J. Powers, J. Lamoree, and S. C. Bhatt, "Characterization of distribution power quality events with Fourier and wavelet transforms," *Power Delivery, IEEE Transactions on*, vol. 15, pp. 247-254, 2000.
- [12] P. Pillay and A. Bhattacharjee, "Application of wavelets to model short-term power system disturbances," *Power Systems, IEEE Transactions on*, vol. 11, pp. 2031-2037, 1996.
- [13] S. Santoso, E. J. Powers, W. M. Grady, and P. Hofmann, "Power quality assessment via wavelet transform analysis," *Power Delivery, IEEE Transactions on*, vol. 11, pp. 924-930, 1996.
- [14] G. T. Heydt and A. W. Galli, "Transient power quality problems analyzed using wavelets," *Power Delivery, IEEE Transactions on*, vol. 12, pp. 908-915, 1997.

- [15] S. Santoso, E. J. Powers, and W. M. Grady, "Power quality disturbance data compression using wavelet transform methods," *Power Delivery, IEEE Transactions on*, vol. 12, pp. 1250-1257, 1997.
- [16] J. Liu and P. Pillay, "An insight into power quality disturbances using wavelet multiresolution analysis," *Power Engineering Review, IEEE*, vol. 19, pp. 59-60, 1999.
- [17] K. Chul Hwan and A. Raj, "Wavelet transforms in power systems. I. General introduction to the wavelet transforms," *Power Engineering Journal [see also Power Engineer]*, vol. 14, pp. 81-87, 2000.
- [18] B. D. Russell, K. Mehta, and R. P. Chinchali, "An arcing fault detection technique using low frequency current components-performance evaluation using recorded field data," *Power Delivery, IEEE Transactions on*, vol. 3, pp. 1493-1500, 1988.
- [19] B. D. Russell and C. L. Benner, "Arcing fault detection for distribution feeders: security assessment in long term field trials," *Power Delivery, IEEE Transactions on*, vol. 10, pp. 676-683, 1995.
- [20] K. L. Butler, B. D. Russell, C. Benner, and K. Andoh, "Characterization of electrical incipient fault signature resulting from tree contact with electric distribution feeders," in *Power Engineering Society Summer Meeting, 1999. IEEE*, 1999, pp. 408-413 vol.1.
- [21] J. S. Bowers, A. Sundaram, C. L. Benner, and B. D. Russell, "Outage avoidance through intelligent detection of incipient equipment failures on distribution feeders," in *Power and Energy Society General Meeting - Conversion and Delivery of Electrical Energy in the 21st Century, 2008 IEEE*, 2008, pp. 1-7.
- [22] G. Kaiser, *A friendly guide to wavelets*. Boston: Birkhäuser, 1994.
- [23] G. Strang and T. Nguyen, *Wavelets and filter banks*. Wellesley, MA: Wellesley-Cambridge Press, 1996.
- [24] F. H. Magnago and A. Abur, "Fault location using wavelets," *Power Delivery, IEEE Transactions on*, vol. 13, pp. 1475-1480, 1998.
- [25] Y. Xiaoguang, C. Bruni, D. Cheung, M. Yiming, G. Sokol, K. Miu, and C. Nwankpa, "Setup of RDAC-a reconfigurable distribution automation and control laboratory," in *Power Engineering Society Summer Meeting, 2001. IEEE*, 2001, pp. 1524-1529 vol.3.
- [26] Z. C. Boulos A., Mai C., "Multi-Purpose Inductive Device for Loading and Fault Experiments," 2005.

Appendix A: Experimental Hardware Setups

This section presents all loading distributions and the corresponding measurement locations. In addition, the fault locations are shown, where all 11 types of faults considered in this work were created. The first section shows the experimental setups used to select the threshold values for the balanced High loading level. Several measurement schemes were used and are tabulated in Table A.1.

The second section presents the experimental setups for validating the threshold values for the balanced High loading level. Specific measurement locations are represented by an M above the respective bus. The Roman numeral I-IV denote the respective DAQ cards utilized for measurements.

Section three shows the experimental setups used for selecting the threshold values for the unbalanced High, Medium and Low load levels. In the event that several measurement schemes were used, or the number of light bulbs used for the High, Medium or Low loading levels had changed, the information is tabulated below the corresponding figure. The final section presents the setups used to validate the performance of the threshold values for the unbalanced High, Medium and Low load levels.

A.1 Experimental Setups Used for Selecting Threshold Values for the Balanced High Loading Level

The load distributions presented in Figure A.1-A3 were performed using 5 parallel connected light bulbs for each load, including the RL equivalent motor load. All 11 fault types were created at each fault location. Four measurement schemes were used for each

of the load distributions and are tabulated in Table A.1. The resulting number of experiments from these three loading distributions was 2112 and were used to select the threshold values for Phase A, B and C.

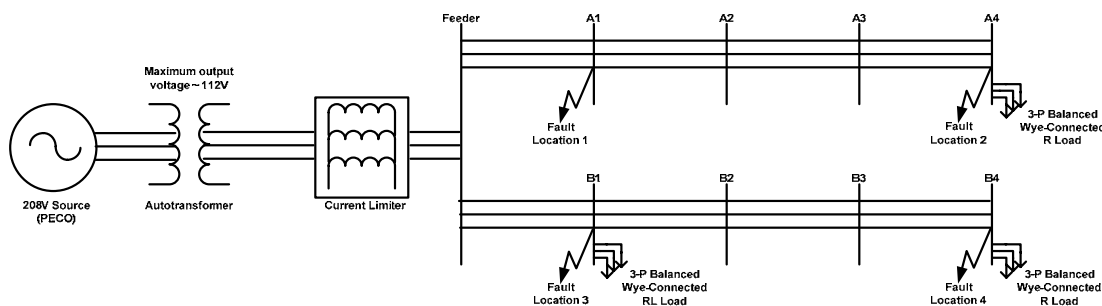


Figure A.1: Configuration 1 for selecting threshold values for the balanced High loading level.

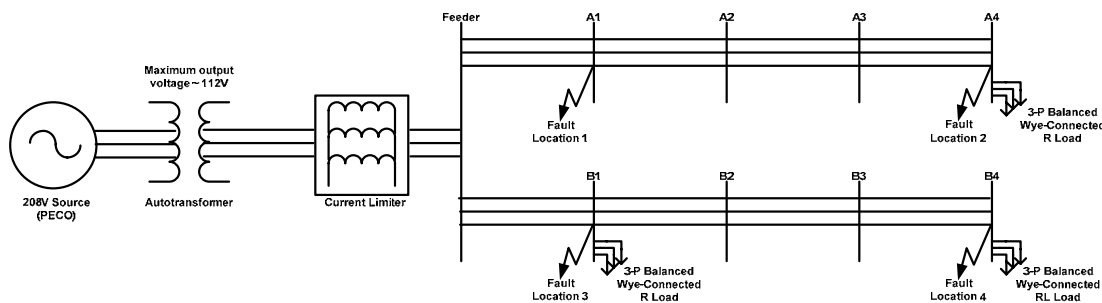


Figure A.2: Configuration 2 for selecting threshold values for the balanced High loading level.

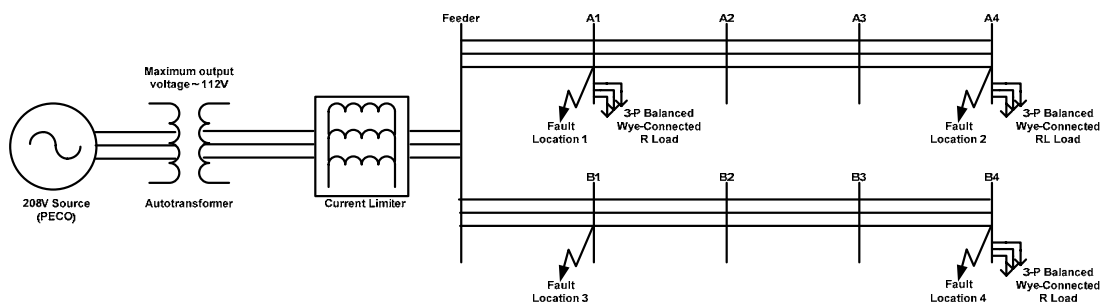


Figure A.3: Configuration 3 for selecting threshold values for the balanced High loading level.

Table A.1: Measurement schemes used for each load distribution in Figure A.1-A.3.

Measurement Scheme	Measurement Locations			
1	F-I	A1-II	A4-III	B1-IV
2	F-I	A1-II	A4-III	B4-IV
3	F-I	A1-IV	B1-II	B4-III
4	F-I	A4-IV	B1-II	B4-III

A.2 Experimental Setups Used for Validating Threshold Values for the Balanced High Loading Level

A new set of load distributions was chosen in order to validate the performance of the threshold values for Phase A, B and C. Again, 5 parallel connected light bulbs were used for each load, including the RL equivalent motor load. Figure A.4 used four different measurement schemes, which are tabulated in Table A.2.

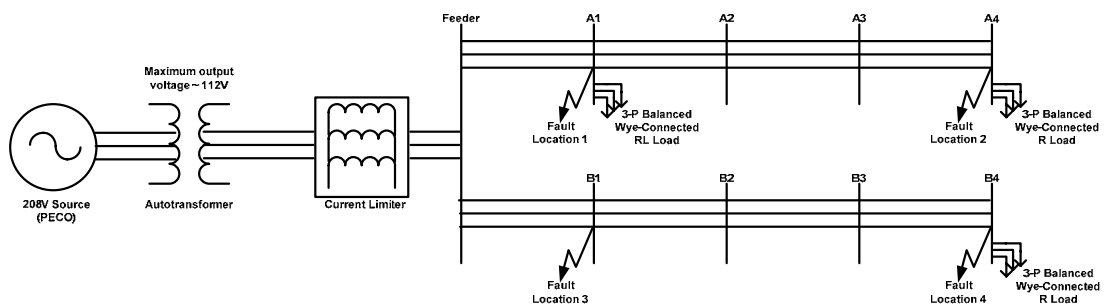
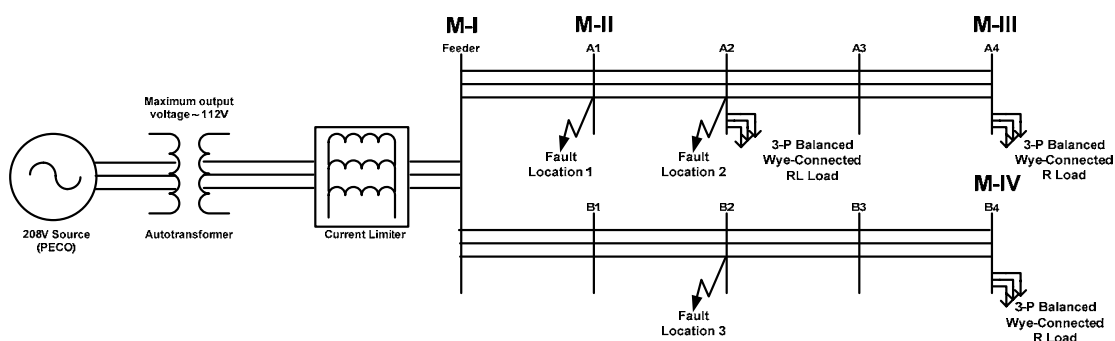
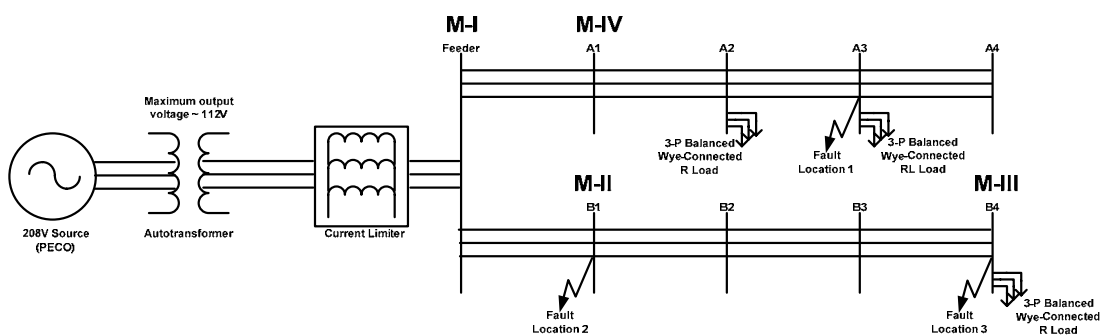
**Figure A.4:** Configuration 1 for validating threshold values for the balanced High loading level.

Table A.2: Measurement schemes used for the load distribution in Figure A.4

Measurement Scheme	Measurement Locations			
1	F-I	A1-II	A4-III	B1-IV
2	F-I	A1-II	A4-III	B4-IV
3	F-I	A1-IV	B1-II	B4-III
4	F-I	A4-IV	B1-II	B4-III

Measurement locations for the load distributions in Figure A.5-A.8 are represented by an M and a Roman numeral above the respective buses. The Roman numeral corresponds to the DAQ card used to collect the measurements.

**Figure A.5:** Configuration 2 for validating threshold values for the balanced High loading level.**Figure A.6:** Configuration 3 for validating threshold values for the balanced High loading level.

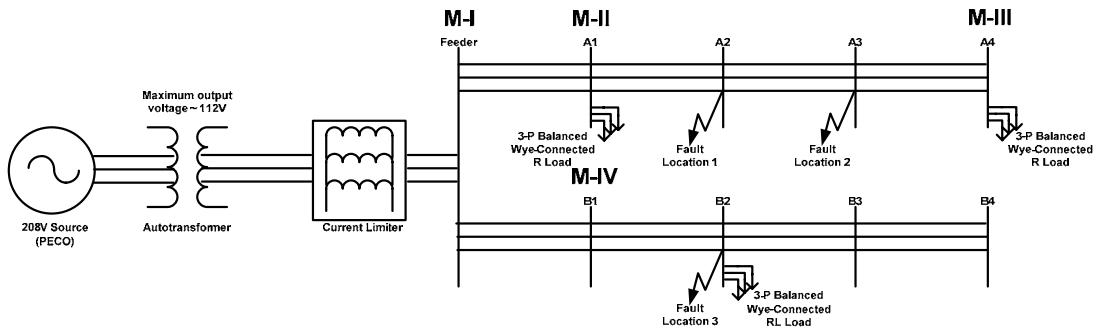


Figure A.7: Configuration 4 for validating threshold values for the balanced High loading level.

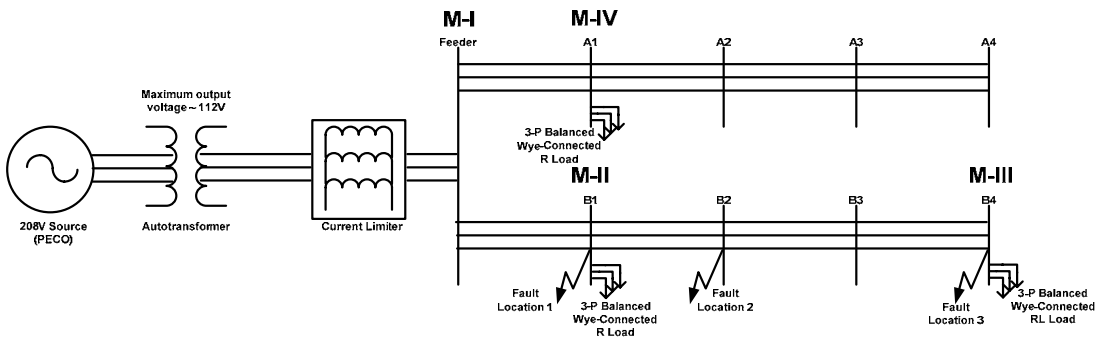


Figure A.8: Configuration 5 for validating threshold values for the balanced High loading level.

A.3 Experimental Setups Used for Selecting Threshold Values for the Unbalanced High, Medium and Low Loading Levels

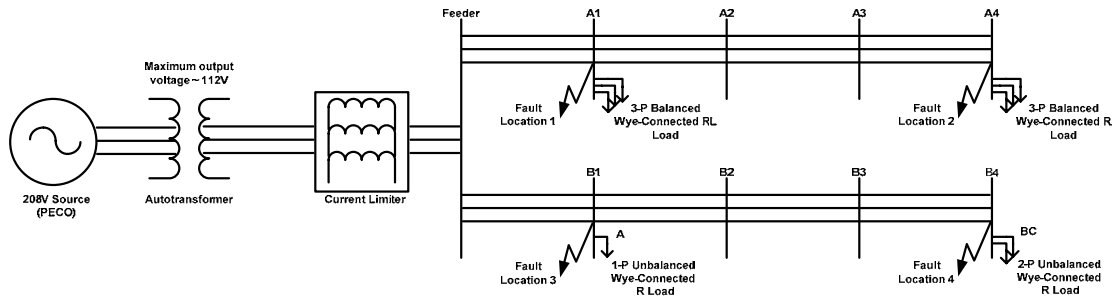


Figure A.9: Configuration 1 for selecting threshold values for the unbalanced High, Medium and Low loading levels.

Table A.3: Measurement schemes used for the load distribution in Figure A.9.

Measurement Scenario	Measurement Locations			
1	F-I	A1-II	A4-III	B1-IV
2	F-I	A1-II	A4-III	B4-IV
3	F-I	A1-IV	B1-II	B4-III
4	F-I	A4-IV	B1-II	B4-III

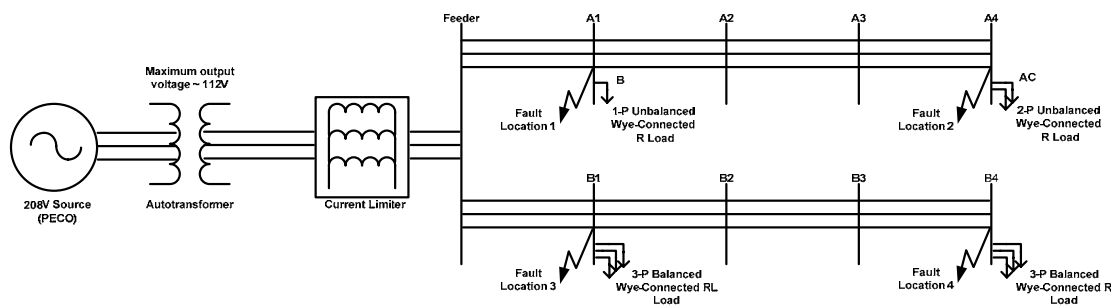


Figure A.10: Configuration 2 for selecting threshold values for the unbalanced High, Medium and Low loading levels.

Table A.4: Measurement schemes used for the load distribution in Figure A.10

Measurement Scenario	Measurement Locations			
1	F-I	A1-II	A4-III	B1-IV
2	F-I	A1-II	A4-III	B4-IV

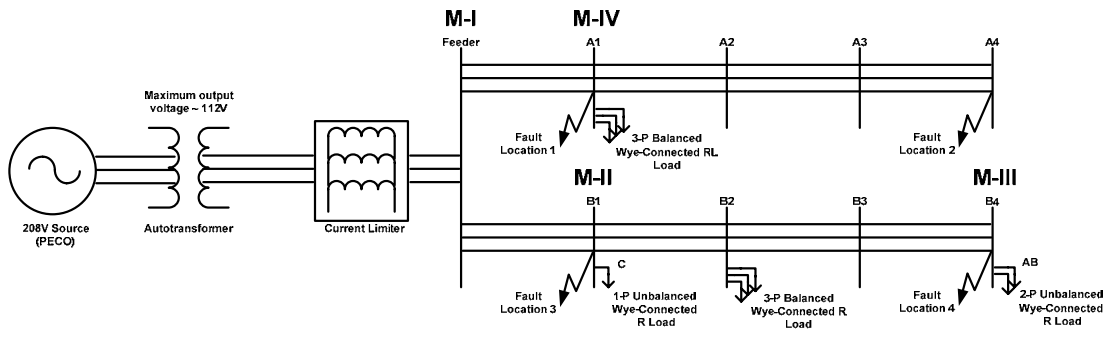


Figure A.11: Configuration 3 for selecting threshold values for the unbalanced High, Medium and Low loading levels.

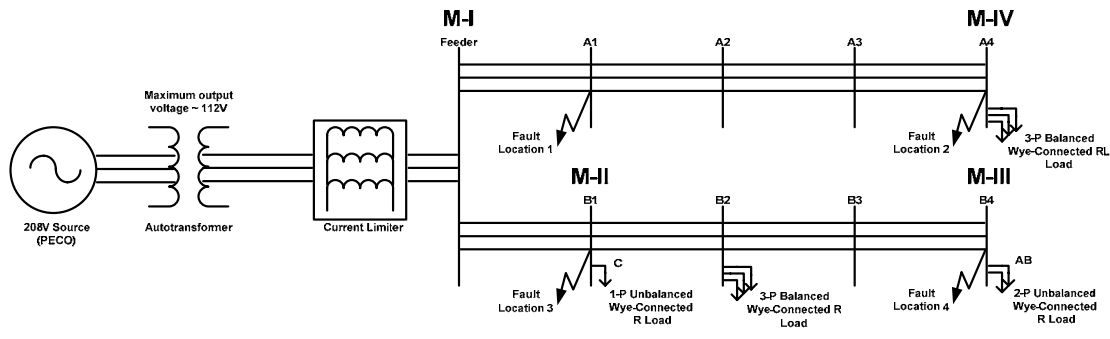


Figure A.12: Configuration 4 for selecting threshold values for the unbalanced High, Medium and Low loading levels.

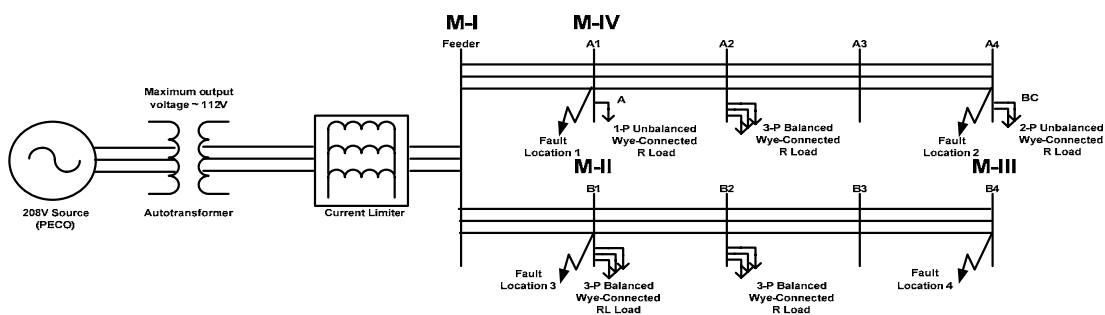


Figure A.13: Configuration 5 for selecting threshold values for the unbalanced High, Medium and Low loading levels.

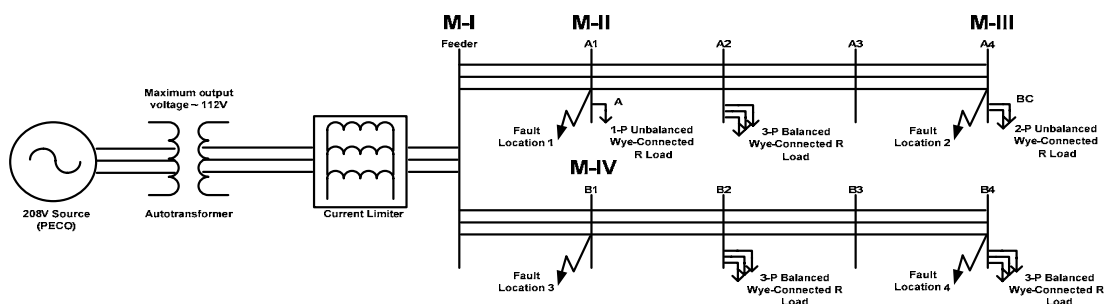


Figure A.14: Configuration 6 for selecting threshold values for the unbalanced High, Medium and Low loading levels.

Table A.5: Number of light bulbs used per phase for each load in Figure A.13-A.14 for the unbalanced High, Medium and Low loading levels.

Bus	A1	A2	A4	B2	B4
Number of Light Bulbs (HIGH)	5 (1-II)	3 (1-I, 2-I)	5 (2-II)	3 (3-II)	5 (3-I)
Number of Light Bulbs (MEDIUM)	3 (1-II)	2 (1-I, 2-I)	3 (2-II)	2 (3-II)	5 (3-I)
Number of Light Bulbs (LOW)	1 (1-II)	1 (1-I, 2-I)	1 (2-II)	1 (3-II)	5 (3-I)

A.4 Experimental Setups Used for Validating Threshold Values for the Unbalanced High, Medium and Low Loading Levels

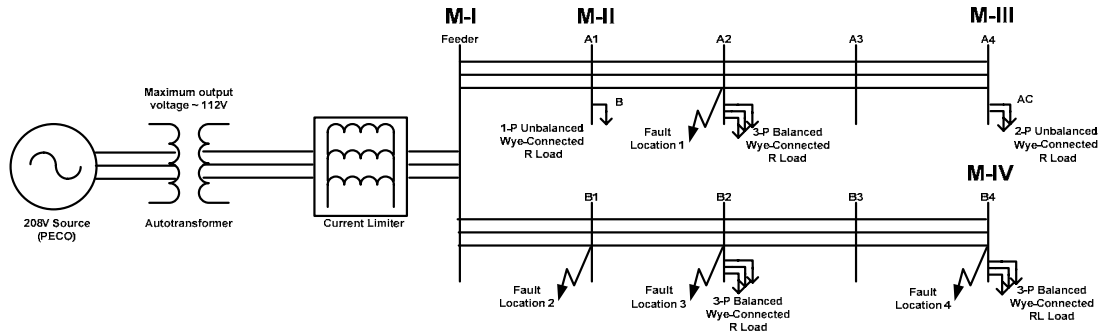


Figure A.15: Configuration 1 for validating threshold values for the unbalanced High, Medium and Low loading levels.

Table A.6: Number of light bulbs used per phase for each load in Figure A.15 for the unbalanced High, Medium and Low loading levels.

Bus	A1	A2	A4	B2	B4
Number of Light Bulbs (HIGH)	5 (1-II)	3 (1-I, 2-I)	5 (2-II)	3 (3-I)	5 (3-II)
Number of Light Bulbs (MEDIUM)	3 (1-II)	2 (1-I, 2-I)	3 (2-II)	2 (3-I)	5 (3-II)
Number of Light Bulbs (LOW)	1 (1-II)	1 (1-I, 2-I)	1 (2-II)	1 (3-I)	5 (3-II)

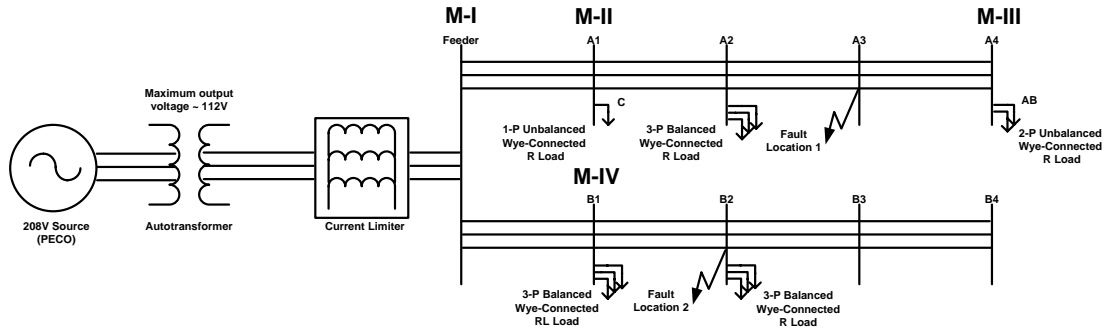


Figure A.16: Configuration 2 for validating threshold values for the unbalanced High, Medium and Low loading levels.

Table A.7: Number of light bulbs used per phase for each load in Figure A.16 for the unbalanced High, Medium and Low loading levels.

Bus	A1	A2	A4	B1	B2
Number of Light Bulbs (HIGH)	5 (1-II)	3 (1-I, 2-I)	5 (2-II)	3 (3-I)	5 (3-II)
Number of Light Bulbs (MEDIUM)	3 (1-II)	2 (1-I, 2-I)	3 (2-II)	2 (3-I)	5 (3-II)
Number of Light Bulbs (LOW)	1 (1-II)	1 (1-I, 2-I)	1 (2-II)	1 (3-I)	5 (3-II)

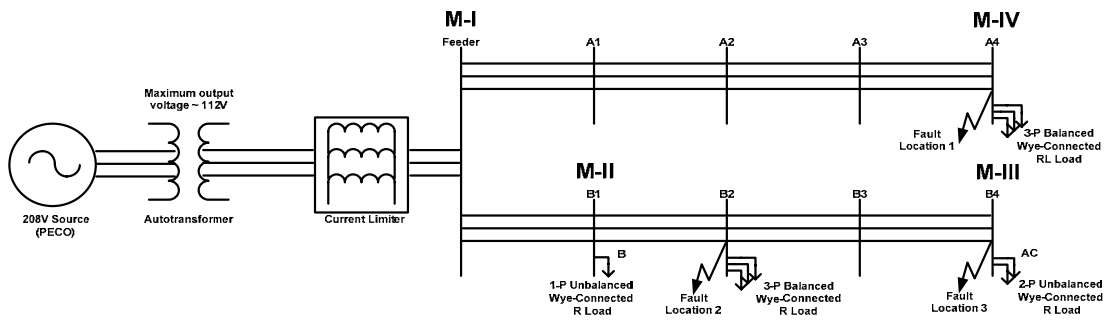


Figure A.17: Configuration 3 for validating threshold values for the unbalanced High, Medium and Low loading levels.

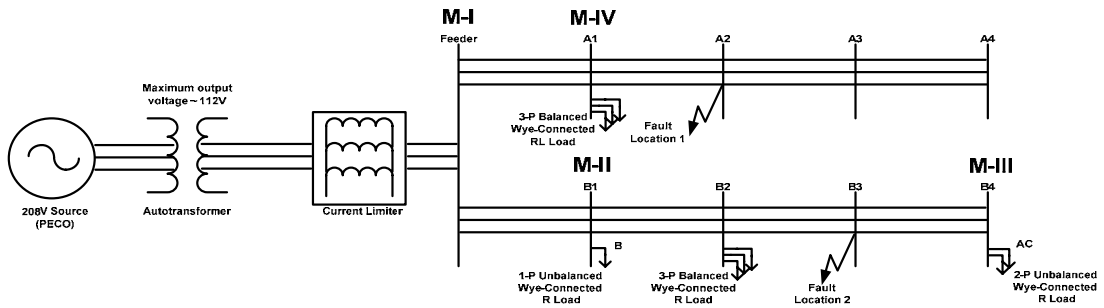


Figure A.18: Configuration 4 for validating threshold values for the unbalanced High, Medium and Low loading levels.

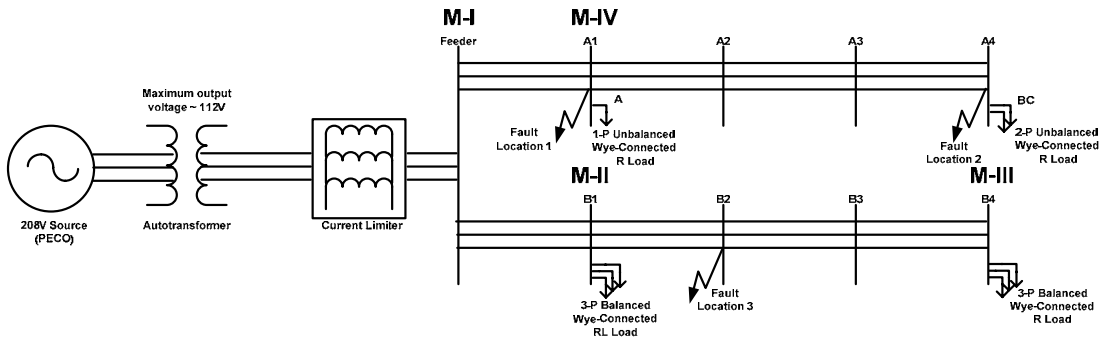


Figure A.19: Configuration 5 for validating threshold values for the unbalanced High, Medium and Low loading levels.

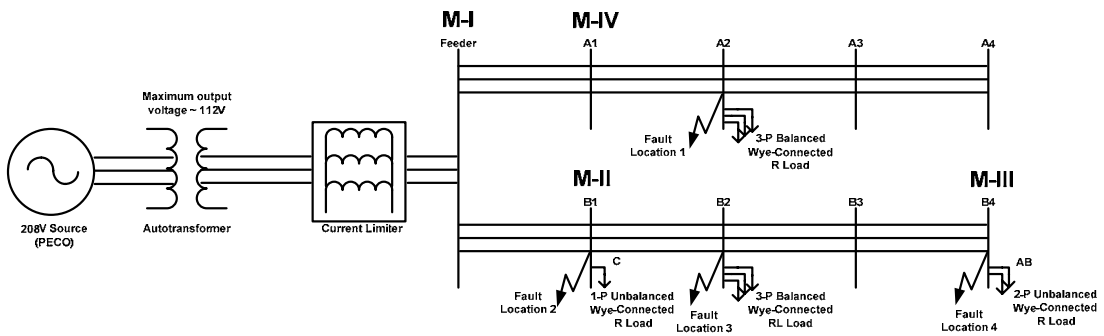


Figure A.20: Configuration 6 for validating threshold values for the unbalanced High, Medium and Low loading levels.

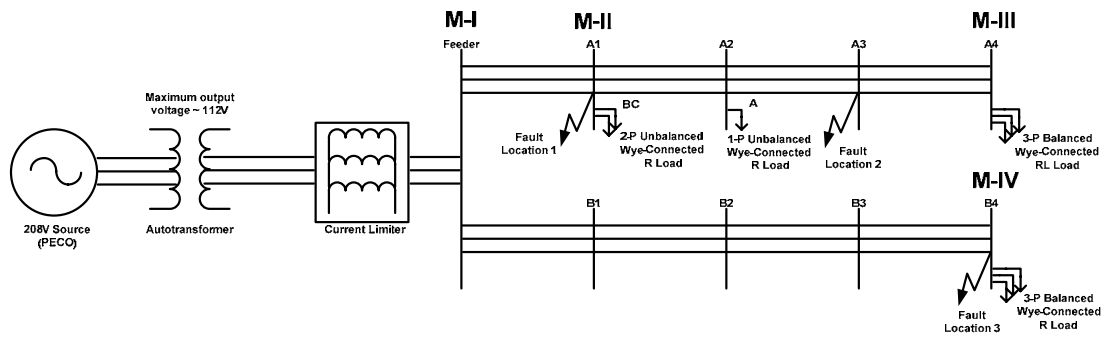


Figure A.21: Configuration 7 for validating threshold values for the unbalanced High, Medium and Low loading levels.

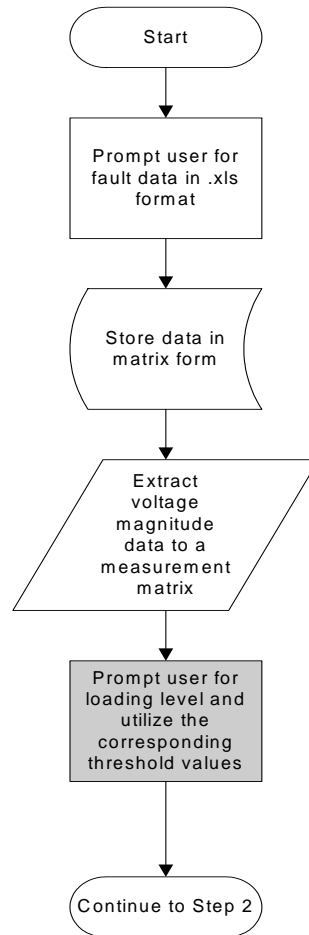
Appendix B: Flowchart for the Wavelet-Based Fault Detector Code

Figure B.1: Step 1 of the wavelet-based fault detection and identification algorithm: data acquisition and preprocessing.

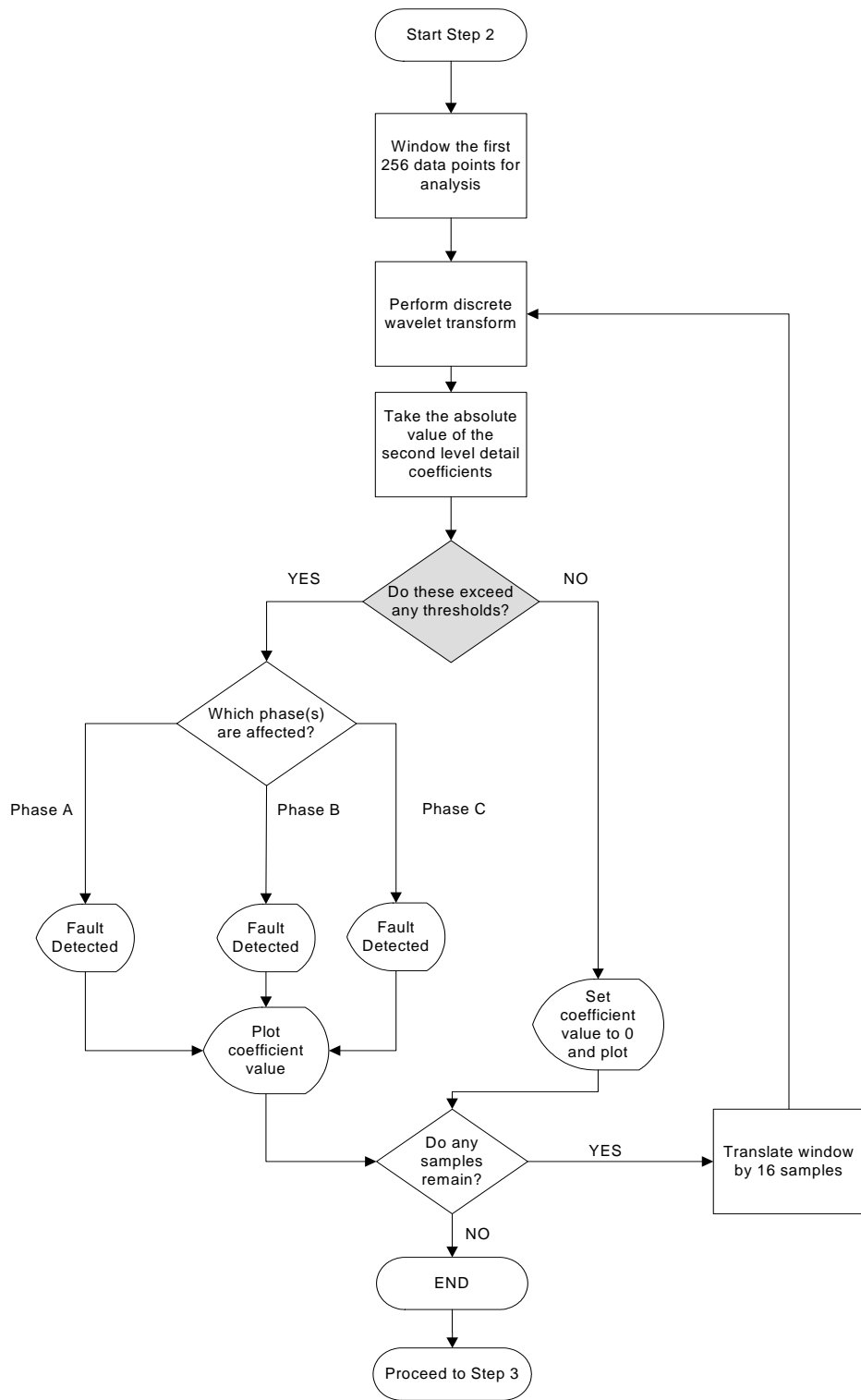


Figure B.2: Step 2 of the wavelet-based fault detection and identification algorithm: fault detection, identification and display of the voltage waveform and wavelet coefficients.

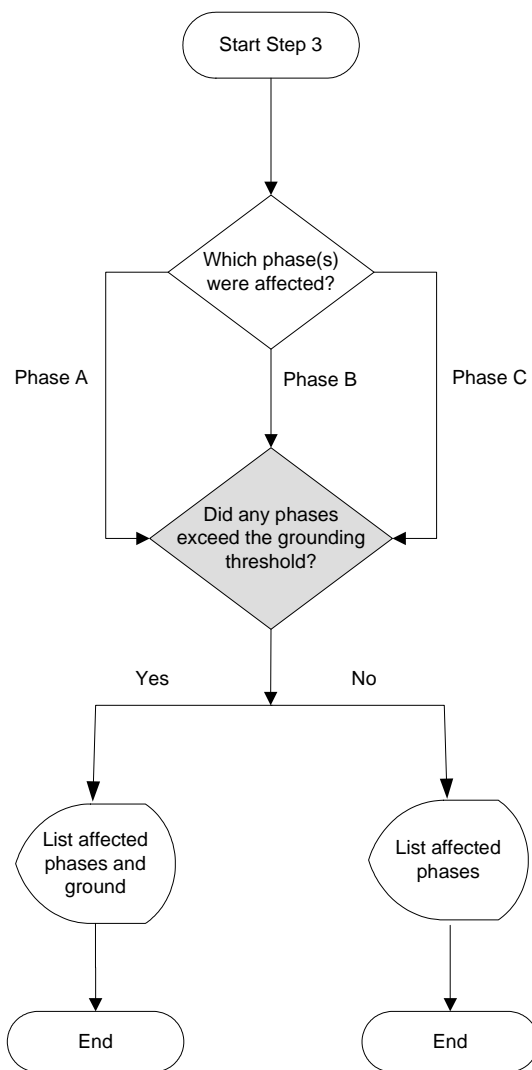


Figure B.3: Step 3 of the wavelet-based fault detection and identification algorithm: grounding determination and output of fault information to the user.